Experimental calibration of Forsterite-Anorthite-CaTschermak-Enstatite (FACE) geobarometer for mantle peridotites

P. Fumagalli[1], G. Borghini[1], E. Rampone[2], S. Poli[1],

[1]Dipartimento di Scienze della Terra, Università di Milano, via Mangiagalli 34, 20133 Milano, Italy

[2] *DISTAV*, Università di Genova, Corso Europa 26, 16132 Genova, Italy

http://dx.doi.org/10.1007/s00410-017-1352-2

Corresponding Author:

Patrizia Fumagalli
Dipartimento di Scienze della Terra « Ardito Desio »
Università degli Studi di Milano
Via Botticelli 23
20133 Milano (Italy)
Email: patrizia.fumagalli@unimi.it

Keywords:

Plagioclase peridotites, geobarometer, mantle exhumation, oceanic lithosphere

Abstract

The crystallization of plagioclase-bearing assemblages in mantle rocks is witness of mantle exhumation at shallow depth. Previous experimental works on peridotites have found systematic compositional variations in coexisting minerals at decreasing pressure within the plagioclase stability field. In this experimental study we present new constraints on the stability of plagioclase as a function of different Na_2O/CaO bulk ratio and we present a new geobarometer for mantle rocks. Experiments have been performed in a single stage piston cylinder at 5-10 kbar, 1050-1150°C at nominally anhydrous conditions using seeded gels of peridotite compositions (Na_2O/CaO=0.08-0.13; X_{Cr}=Cr/(Cr+Al)= 0.07-0.10) as starting materials. As expected, the increase of bulk Na_2O/CaO ratio extends the plagioclase stability to higher pressure; in the studied High-Na Fertile Lherzolite (HNa-FLZ) the plagioclase-spinel transition occurs at 1100°C between 9-10 kbar; in a fertile lherzolite (FLZ) with Na_2O/CaO = 0.08 it occurs between 8-9 kbar, at 1100°C. This study provides, together with previous experimental results, a consistent database, covering a wide range of P-T conditions (3-9 kbar, 1000-1150°C) and variable bulk compositions, to be used to define and calibrate a geobarometer for plagioclase-bearing mantle rocks. The pressure sensitive equilibrium:

$$Mg_2SiO_4\ ^{Ol} + CaAl_2Si_2O_8\ ^{Pl} = CaAl_2SiO_6\ ^{Cpx} + Mg_2Si_2O_6\ ^{Opx}$$

Forsterite Anorthite Ca-Tschermak Enstatite

has been empirically calibrated by least squares regression analysis of experimental data combined with Monte Carlo simulation. Result of the fit gives the following equation:

$$P = 7.2\ (\pm 2.9) + 0.0078\ (\pm 0.0021)\ T + 0.0022\ (\pm 0.0001)\ T \ln K$$

$$R^2 = 0.93$$

where P is expressed in kbar, temperature in kelvin, K is the equilibrium constant $K = a_{Ca\text{-}Ts} * a_{en} / a_{an} * a_{fo}$, where $a_{Ca\text{-}Ts}$, a_{en}, a_{an}, a_{fo} are the activities of Ca-Tschermak in clinopyroxene, enstatite in orthopyroxene, anorthite in plagioclase and forsterite in olivine. The proposed geobarometer for plagioclase peridotites, coupled to detailed microstructural and mineral chemistry investigations, represents a valuable tool to track the exhumation of the lithospheric mantle at extensional environments.

INTRODUCTION

Plagioclase-bearing mantle peridotites are a widespread component in the oceanic lithosphere formed at slow and ultra-slow spreading ridge settings and passive margins (e.g. Dick and Bullen 1984; Hamlyn and Bonatti 1980; Bonatti et al. 1986; Kornprobst and Tabit 1988; Dick 1989; Cannat and Seyler 1995; Tartarotti et al. 2002; Chazot et al. 2005; Cannat et al. 2006; Kelemen et al. 2007; Tamura et al. 2008; Dick et al. 2010; Warren and Shimizu 2010; Brunelli and Seyler 2010; Martin et al. 2014a, b; Secchiari et al. 2016; Warren 2016), where km-scale sectors of lithospheric mantle are tectonically exposed at the ocean floor along extensional detachments (e.g. Beslier et al. 1993; Michael et al. 2003; Manatschal 2004; Müntener et al. 2004; Manatschal and Müntener 2009). Plagioclase formation in these mantle peridotites can be related either to open-system magmatic processes, i.e. percolation and impregnation by basaltic melts, or to close-system metamorphic subsolidus recrystallization.

In spite of their different origin, the crystallization of (plagioclase + olivine)-bearing equilibrium assemblages in peridotites is generally considered witness of mantle exhumation at shallow (< 10 kbar) lithospheric depths (e.g. Green 1964; Obata 1980; Rampone et al. 1993, 1997, 2005, 2008; Ozawa & Takahashi 1995; Furusho and Kanagawa 1999; Newmann et al. 1999; Piccardo et al. 2004, 2007; Piccardo and Vissers 2007; Chazot et al. 2005; Montanini et al. 2006; Müntener and Manatschal 2006; Borghini et al., 2007; Müntener et al. 2010; Hidas et al. 2013). The estimate of the equilibration pressure of plagioclase-facies peridotites is therefore relevant to track the geodynamic evolution of lithospheric mantle at extensional settings. Despite this significance, no reliable geobarometers are available so far to be applied to ultramafic rocks in this pressure-temperature realm.

A number of experimental studies, mostly focused on simple CaO-MgO-Al_2O_3-SiO_2 (CMAS) and Na_2O-CMAS (NCMAS) systems, have pointed out that at subsolidus conditions plagioclase lherzolite assemblages are stable up to 10 kbar (Kushiro and Yoder 1966; Green and Hibberson 1970; Obata 1976; Herzberg 1978; Presnall et al. 1979; Gasparik 1984; Walter and Presnall 1994). Subsolidus experimental data in the complex chemical system TiO_2, Cr_2O_3, FeO-NCMAS (Ti,Cr-FNCMAS) on depleted and fertile lherzolite compositions (Borghini et al. 2010) documented systematic compositional variations in coexisting minerals at decreasing pressure within the plagioclase stability field, similar to what observed in natural equilibrated plagioclase peridotites. In these experiments, plagioclase composition varies significantly (anorthite=An=Ca/(Ca+Na)=0.59-0.83) in a narrow range of pressure. In a subsequent paper, Borghini et al. (2011) defined the anorthite isopleths in plagioclase as a function of P and T for a

specific fertile lherzolite composition, and they demonstrated that plagioclase-facies equilibrium pressures can be estimated by comparing experimental data on a fertile lherzolite and microstructural-chemical observations in natural samples with the same bulk composition. This method represents a first-order empirical tool to trace the decompressional evolution of the lithospheric mantle up to very low-pressure, potentially applicable to equilibrated plagioclase-facies peridotites of different origin. However, the composition of plagioclase at variable bulk Na_2O/CaO ratios has not been fully discerned yet, limiting this approach to a restricted bulk compositional range.

Thermodynamic modelling of peridotitic systems can rely on several experimental studies considering the effect of additional relevant component such as Cr and Fe (Gasparik 1985, 1987; Klemme 2004). However, when applied to more complex systems (approaching natural peridotite bulk compositions), a detailed evaluation of mineral chemistry variability as a function of pressure failed to reproduce experimental results. In particular, Borghini et al. (2010) experimentally demonstrated that, although thermodynamic Cr solid solutions have been increasingly improved, the prediction of the plagioclase- to spinel- facies transition and the variability of mineral chemistry of major phases such as pyroxene and plagioclase in a pressure range of 2-10 kbar is still far from being reliable. As a result thermodynamic modelling does not enable an accurate estimate of equilibrium pressure of plagioclase-bearing peridotites.

In this paper, we present the results of new experiments on a High-Na Fertile Lherzolite (HNa-FLZ, bulk Na_2O/CaO ratio = 0.13), representative of many refertilized lithospheric peridotites at extensional settings, thus enlarging significantly our investigated compositional spectrum (Na_2O/CaO = 0.08 – 0.13). Major aims of this experimental study are: i) to investigate the effect of Na_2O/CaO ratio on the mineral chemistry variability within the plagioclase stability field, and ii) to enlarge the experimental database available so far, in order to establish and empirically derive a robust geobarometer for plagioclase-bearing mantle peridotites.

We will consider the pressure and temperature dependent reaction

$$Mg_2SiO_4\ ^{Ol} + CaAl_2Si_2O_8\ ^{Pl} = CaAl_2SiO_6\ ^{Cpx} + Mg_2Si_2O_6\ ^{Opx} \quad (1)$$

forsterite anorthite Ca-Tschermak enstatite

which was first reported by Herzberg (1978) as possible univariant equilibrium to be used in geobarometry of plagioclase peridotites in the CMAS system. We will demonstrate that reaction (1) reasonably explains the experimental mineral chemistry variations within the plagioclase stability field in more complex systems (Ti,Cr-FNCMAS), further supporting its relevance as geobarometer. In the following we refer to equilibrium (1) as the Forsterite-Anorthite-CaTschermak-Enstatite (FACE) equilibrium.

Noteworthy, the equilibrium between anorthite and Ca-Tschermak in the presence of quartz has been extensively explored and McCarthy and Patino-Douce (1998) reported an empirical calibration to be used in SiO_2-saturated bulk composition such as gneisses and tonalities (Silica-Ca-Tsckermak-Anorthite – SCAn geobarometer). The geobarometer proposed in this study thus enlarge the knowledge of plagioclase-clinopyroxene chemical equilibria for SiO_2-undersaturated compositions.

In the following paragraphs we will first present the experimental dataset. We will then derive the activity-models for phases involved in equilibrium (1) and discuss the calibration of equilibrium (1). Finally, we will discuss the application of the empirically derived geobarometer to different plagioclase-bearing ultramafic suites.

THE EXPERIMENTAL DATASET

Starting materials

In order to evaluate the effect of Na_2O/CaO bulk ratio on the variations of mineral chemistry within the plagioclase stability field, and enlarge the experimental database to be used as a dataset for geobarometer calibration, we calculated an appropriate bulk composition starting from the fertile lherzolite FLZ (Borghini et al. 2010, 2011), and adding Na_2O up to a Na_2O/CaO = 0.13 (Table 1). The resulting bulk composition (X_{Mg}=MgO/(MgO+FeO_{tot}) = 0.90, X_{Cr} = 0.07) falls within the range of natural bulk peridotites from both oceanic, ophiolitic and orogenic environment (Fig. 1), and together with FLZ and DLZ previously investigated (Borghini et al. 2010, 2011) covers a representative wide compositional range of natural plagioclase-bearing peridotites.

Following previous studies on peridotite compositions, in order to enhance the modal abundance of minor phases, we subtracted 40% olivine (Fo_{90}) to the starting bulk composition. For the sake of completeness, we performed additional experiments using the same bulk composition as in Borghini et al. (2010): a fertile lherzolite (FLZ, X_{Mg} = 0.90, X_{Cr}= 0.07, Na_2O/CaO= 0.08) and a depleted lherzolite (DLZ, X_{Mg} = 0.90, X_{Cr} = 0.10, Na_2O/CaO= 0.09) (see Table 1).

Gels have been used as starting materials. They have been prepared following the method of Hamilton and Henderson (1968), using tetraethylorthosilicate (TEOS) as silica source, tetraethylorthotitanate (TEOT) as titanium source, pure Na-, Ca-, Mg- and Al- nitric solutions, ferric benzoate and ammonium dichromate. Gels were fired in a gas-mixing furnace at 850°C and f_{O2} conditions approaching the FMQ (fayalite-magnetite- quartz) buffer at 1atm, to ensure that the iron was present in the starting composition dominantly as FeO. In order to promote the nucleation of minor phases, we added to the gel 1 wt.% of a mixture of synthetic anorthite (70%) and spinel (30%). Assuming a complete resorption of the seeds, this would increase the Al_2O_3 and CaO

content of about 6.6% and 1.5% respectively, and would decrease the SiO_2 and MgO contents of less than 0.01%. However, in most experiments we found relics of seeds, indicating that the addition of the seed mixture can be considered negligible in terms of deviation of the bulk composition.

Run conditions and apparatus

Subsolidus experiments were performed in a single stage piston cylinder at the Dipartimento di Scienze della Terra in Milano (Italy). Run conditions range from 5 to 10 kbar, and 1050 to 1150°C (Table 2). Although the thermal regime expected in natural plagioclase peridotites extends towards lower temperatures, slow reaction rates in nominally anhydrous conditions prevent experimental investigations at $T \leq 1000$°C. In order to favour crystallization runs lasted up to 1002 hrs. Salt + Pyrex + MgO assemblies and graphite heater were used. Temperature was measured with S-type thermocouples and is considered to be accurate to 5°C. Pressure uncertainties are considered to be ± 3%. An initial load of about 2.5 kbar was applied, then the sample was heated to 400 °C to soften the Pyrex and then compressed to the final run pressure, before heating up to the experimental temperature.

Approximately 20 mg of starting material was loaded into a graphite inner capsule (outer diameter 2.8mm), and then welded into an outer Pt capsule (outer diameter 3.0 mm, length about 7-8 mm). Graphite was used to isolate the sample from the Pt capsule and to avoid Fe loss (Kinzler 1997; Walter 1998). The graphite-Pt assembly (combined with pre-conditioning of the starting material at FMQ) maintained the oxygen fugacity below the graphite-C-O vapor buffer (Ulmer and Luth, 1991). To maintain anhydrous conditions, the capsule plus the starting material and the assembly were dried in an oven at 250°C for at least 12 hrs, before welding and running the experiments.

Run products were initially inspected using backscattered electron (BSE) and secondary electron images. Microprobe analyses were performed using a JEOL JXA 8200 Superprobe equipped with five WDS spectrometers and one energy-dispersive spectrometer -EDS (1 mm beam size; beam conditions 15 kV and 15 nA) at the Dipartimento di Scienze della Terra, University of Milano. Both images and X-ray element maps were extremely useful in textural examination of the experimental charges and selection of point analysis.

Approach to Equilibrium

In complex systems such as those investigated in the present study, and for continuous reactions involving variations in the mineral chemistry of reactants and products, reversals are not

easily made. Therefore, runs of the present studies are unreversed synthesis experiments. However, a number of observations strongly support the attainment of equilibrium and therefore validate the goodness of our experimental results: i) the growth of homogeneous, chemically unzoned mineral phases, favoured by the long run durations (Table 2) ii) coherent and systematic variations in mineral chemistry and element partitioning at variable pressure and temperature conditions, iii) well-developed textures with mineral phases homogeneously distributed in the charges iv) the growth of compositionally homogeneous rims on mineral seeds.

PHASE ASSEMBLAGES AND TEXTURES

Run results and experimental conditions are reported in Table 2. Phase assemblages found in the experimental charges as a function of P and T are shown in Figure 2. Plagioclase is stable in assemblage with olivine, orthopyroxene, clinopyroxene, Cr-rich spinel and it is ubiquitous in all experiments except the one at 10 kbar, 1100°C (Fig. 2). At these conditions, the plagioclase-free assemblage made of olivine, orthopyroxene, clinopyroxene and an Al-rich spinel is stable. Run results on FLZ and DLZ are in agreement with previous experimental studies on the same bulk compositions (Borghini et al. 2010, 2011), which showed that the plagioclase-out boundary occurs between 8 and 9 kbar, at 1100°C in the fertile bulk composition (FLZ) and between 7 and 8 kbar in the depleted bulk (DLZ).

Although care has been taken during the preparation, loading and welding of capsule in order to avoid H_2O contamination, we found traces of amphibole at the microprobe scale in most of the experiments. The evaluation of phase abundances in the run charges is not always possible because of the difficulties in analysing tiny fine-grained phases, such as spinel. However, when the mineral chemistry of all phases is available at the same accuracy level, weighted least squares calculations have been performed. Mass balance results in amphibole abundance ranging from 0.56 (at 9 kbar, 1100°C) to 3.2 wt.% (at 7 kbar, 1100°C). BSE images confirm visually such abundance in all experiments. Assuming a stoichiometric content of hydrogen in the amphibole structure (i.e. 2 wt % H_2O), the amount of H_2O that entered the capsule can be estimated between 0.01 to 0.06 wt %. Whether this happened while welding or during the run, as a result of hydrogen permeability of the assembly, is difficult to assess.

Most of the experiments show well-developed textures. The occurrence of numerous triple junctions involving olivine, pyroxenes and plagioclase suggest well-equilibrated textures (Fig. 3). Higher temperatures enhanced larger grain size: at 1150 °C, grain size can reach up to 10μm (Fig. 3a), while at temperature of only 50°C lower, in spite of longer run durations, crystals rarely reach 10 μm of size, being mostly between 2 and 5 μm (Fig. 3b). At 6.5 kbar and 1050°C (run LC4), the

extremely fine grain-size texture prevented satisfactory chemical analysis of mineral phases; therefore although the assessment of the phase assemblage have been derived with the help of EDS spectra, accurate chemical analysis are not available for run LC4.

Olivine generally occurs as 2-8 μm-sized grains, with euhedral to subhedral habit. It is recognizable from orthopyroxene mainly by EDS or X-ray element mapping, as in BSE images olivine presents only a very slightly lighter contrast with respect to orthopyroxene. On the contrary, clinopyroxene shows a very bright contrast in BSE images, and it mainly occurs as euhedral crystals of up to 10-12 μm size. Plagioclase is homogenously distributed in the run charges; it occurs as small, anhedral crystals ranging from 2 to 5 μm, and it is interstitial between olivine and pyroxenes grains. In plagioclase-bearing phase assemblages, spinels occur both in the matrix and included in plagioclase. They are newly crystallized small rounded bright spinels that can reach, in the higher temperature runs, up to about 5 μm of size (Fig. 3b,c). However, in most cases spinels are too small to allow reliable compositional analysis (see for example Fig. 3a).

The plagioclase-free phase assemblage obtained at 10 kbar, 1100°C presents very similar textural relations involving olivine and pyroxenes. Spinels are homogenously distributed but extremely tiny in size making their analysis extremely difficult.

MINERAL CHEMISTRY

Most *olivines* present an X_{Mg} value variable from 0.89 to 0.90, reflecting the bulk compositions (Table 3 and Supplementary Material ST1). No relevant correlation with pressure and temperature has been recognized, suggesting that olivine composition remains relatively constant within the stability field of plagioclase. In experiment LC1b (5.5 kbar, 1100°C, run duration 502 hrs), we could not obtain reliable analysis of olivine, due to extremely fine-grained texture.

Clinopyroxenes show quite uniform X_{Mg} values, ranging from 0.90 to 0.91, in agreement with the bulk compositions (Table 3 and Supplementary Material ST2). On the other hand, Na, Al, and Cr abundances display significant pressure-dependent variations. In the HNa-FLZ bulk composition, Na increases from 0.032 a.p.f.u. at the lowest pressure investigated (5 kbar, 1100°C), up to 0.079 a.p.f.u. in the plagioclase-free domain (10 kbar, 1100°C), suggesting not only a jadeite increase (and anorthite decrease) at the plagioclase-out boundary, but also a continuous variation within the plagioclase-facies stability field. Na content of clinopyroxene in FLZ and DLZ bulk are 0.039 (7 kbar, 1150°C) and 0.029 (5.5 kbar, 1100°C) respectively, i.e. slightly lower than the Na contents in clinopyroxene at the same P-T conditions in the HNa-FLZ bulk. Ca is rather constant, resulting in a Ca/(Ca+Na) ratio that is only slightly decreasing with pressure (squares in Fig. 4). This is in perfect agreement with previous experimental results (Borghini et al. 2010). As expected,

Al content in clinopyroxene is positively correlated with pressure, increasing from 0.183 a.p.f.u. at 5 kbar, 1100°C to 0.286 a.p.f.u. at 9 kbar, 1100°C in the HNa-FLZ bulk composition (Fig. 5a). This trend is perfectly aligned with previous experiments on different bulk compositions. Remarkably the Al content in clinopyroxenes in HNa-FLZ overlaps that of clinopyroxene in FLZ, whereas significant lower values are observed in clinopyroxene of DLZ (Fig. 5a). This suggests that bulk X_{Cr} rather than Na_2O/CaO influences alumina solubility in clinopyroxene. Cr is rather constant with pressure, mostly 0.020-0.031 a.p.f.u. in the HNa-FLZ. As a result, the X_{Cr} value [=Cr/(Cr+Al^{VI})] slightly decreases with pressure (Supplementary Material ST2).

Orthopyroxenes have X_{Mg} values ranging 0.89-0.90, consistent with the bulk compositions, and do not exhibit significant variations as a function of pressure and temperature conditions (Table 3 and Supplementary Material ST3). As observed for clinopyroxene, the most striking compositional change in orthopyroxenes within the plagioclase stability field is the pressure dependence of Al content, this latter ranging from 0.140 a.p.f.u. at 5 kbar, 1100°C to 0.232 a.p.f.u at 10 kbar, 1100°C in the HNa-FLZ bulk composition (Fig. 5b). The Al contents of orthopyroxenes in experiments on DLZ and FLZ bulk compositions define consistent trends (Fig. 5b). As observed in clinopyroxenes, Cr abundances in orthopyroxenes are rather low, ranging from 0.015 to 0.020 a.p.f.u. in the HNa-FLZ bulk composition. As a result, the X_{Cr} values slightly decrease with pressure (Supplementary Material ST3).

Despite many efforts in deriving new thermodynamic models for Cr-bearing phases (Klemme, 2004; Fumagalli and Klemme, 2015 for a review) some discrepancies still exist when dealing with complex systems. The Cr/(Cr+Al^{VI}) values in pyroxenes derived in the present study are compared with the results of thermodynamic modelling in Figure 1S of the Supplementary Material. It is evident that present thermodynamic data underestimate the Cr content in pyroxenes and this results in an overestimation of Cr contents in spinel. A possible explanation to this discrepancy is the fact that Ca is not considered in the solid solution model for orthopyroxene. However, a thorough discussion of this specific aspect is beyond the scope of this study.

Plagioclases exhibit an anorthite content (X_{An} = Ca/(Ca+Na)) strongly correlated with pressure (Fig. 4). It decreases from 0.69 at 5 kbar, 1100°C, down to 0.51 at 9 kbar, 1100°C (Fig. 4). At fixed pressure of 7 and 8 kbar, the similar or slightly higher anorthite contents of plagioclase in the runs at 1150°C with respect to 1100°C confirm a minor positive correlation with temperature (Table 3 and Supplementary Material ST4). The composition of plagioclase in experiments on HNa-FLZ are, therefore, strikingly comparable with previous results on the DLZ and FLZ bulk compositions at similar P-T conditions, as also corroborated by the additional experiments on DLZ and FLZ performed in this study (Fig. 4, Table 3). In particular, these results revealed that, although

plagioclase stability expands to higher pressure as bulk Na_2O/CaO ratio increases, its composition is not significantly influenced by the Na_2O/CaO ratio of the bulk in the range of peridotite compositions here investigated.

The extremely small size of *spinels* allowed only few chemical analyses. However, available data are in agreement with previous results of Borghini et al. (2010) (Table 3 and Supplementary Material ST5). In the HNa-FLZ bulk composition, spinels show an increase of X_{Mg} (from 0.77 at 6 kbar, 1100°C to 0.82 at 9 kbar, 1100°C) correlated with a decrease in X_{Cr} (from 0.236 at 6 kbar, 1100°C to 0.064 at 9 kbar, 1100°C). No significant chemical variations are observed between spinels included in plagioclase and spinels in the matrix.

As previously mentioned, trace amounts of amphibole have been found in the run charges. Amphiboles are mainly pargasites (Leake et al. 1997). Their Ca/(Ca+Na) ratios are slightly decreasing with increasing pressure (from 0.68 to 0.62 at 5 kbar, 1100°C and 9 kbar, 1100°C respectively; Supplementary Material ST6), following the Ca,Na partitioning of the coexisting alkali-bearing phases, i.e. plagioclase and clinopyroxene (Fig. 4).

LOCATION OF THE PLAGIOCLASE- TO SPINEL- FACIES TRANSITION

Although the present study is not devoted to locate the plagioclase-facies to spinel-facies boundary, the experiment at 10 kbar, 1100°C allows us to predict the effect of Na_2O/CaO ratio and X_{Cr} on the transition, by comparing our results with previous experimental data performed on different bulk compositions.

Our study indicates that the disappearance of plagioclase in fertile lherzolite HNa-FLZ occurs between 9 and 10 kbar at 1100°C. Borghini et al. (2010) discussed the role of bulk chemistry on the pressure of plagioclase-out boundary in lherzolite compositions. Plagioclase stability in lherzolites is mostly controlled by CIPW normative albite/diopside ratio (Ab/Di) and X_{Cr} in the whole rock (Green and Hibberson 1970; Green and Falloon 1998; Borghini et al. 2010). Available experimental data offer the possibility of comparing a wide range of bulk compositions: among lherzolites, HNa-FLZ have the same X_{Cr} as FLZ, but significantly higher Ab/Di ratio (Table 1, Fig. 6), thus allowing to evaluate the effect of the bulk Na_2O/CaO. The increase of albite component in plagioclase moves the plagioclase- to spinel-facies transition to pressure higher than about 10 kbar (Fig. 6). Indeed, in pyrolites such as MORB Pyrolite (MPY) and Hawaiian Pyrolite (HPY) having higher Ab/Di ratio than lherzolites, plagioclase persists at even higher pressure (Niida and Green 1999; Green and Falloon 1998). The effect of X_{Cr} on the transition is opposite: an increase of X_{Cr} lowers the transition, expanding the stability of spinel as observed for the depleted lherzolite (DLZ).

The stability of plagioclase and its persistence at higher pressure is therefore a balance between these two opposite effects.

REGRESSION MODEL

The experimental dataset previously presented shows a striking relation between anorthite component in plagioclase and the X_{Al}^{M1} in clinopyroxene (Fig. 7). The diagram confirms and quantitatively proves that, as pressure increases, the anorthite content in plagioclase decreases while the X_{Al}^{M1} in clinopyroxene increases, in agreement with the P,T dependent equilibrium (1). Our results confirm the correlation reported by Borghini et al. (2010, 2011 over a wide range of peridotite bulk composition (Na_2O/CaO from 0.08-0.13; X_{Cr} from 0.07-0.10). The reaction (1) is therefore a potential geobarometer for mantle rocks. Remarkably, the correlation appears to be uninfluenced by the different Na_2O/CaO ratio of the investigated bulks.

A limited number of experimental studies on mantle compositions at P and T conditions of interest are available with comparable detailed mineral chemistry acquisition, mainly because they were devoted to melting relations rather than subsolidus variations in mineral chemistry of solid phases (Falloon et al. 1997; Niida and Green 1999; Chalot-Prat et al. 2010, 2013). These studies do not provide systematics on the mineral chemistry of equilibrium subsolidus phase assemblages, rather they aim to present data on crystallization/melting and peridotite reaction experiments starting from mixed melt-peridotite compositions. In particular, Falloon et al. (1997) found, in experiments at 10 kbar, a rather variable plagioclase anorthite content (X_{an} ranging 0.68-0.55) associated with a constant X_{Al}^{M1} in clinopyroxene. Similarly, Chalot-Prat et al. (2010, 2013) report at 75 kbar and 1180-1240°C plagioclases that span over a wide range of composition (X_{an} ranging from 0.95 to 0.5) coupled with rather constant X_{Al}^{M1} = 0.10 in clinopyroxene (Fig. 7). The complexity of starting bulk compositions in Chalot-Prat et al. (2010, 2013), together with the peculiar experimental set up with layered capsules used in their experiments and in those of Faloon et al. (1997), do not allow comparison and evaluation of phase relations. Accordingly, these data were not taken into account for the calibration of the geobarometer.

For the FACE equilibrium (1) we have:

$$- RT \ln K = \Delta H - P\Delta V + T\Delta S$$

where $K = a_{Ca\text{-}Ts} * a_{en} / a_{fo} * a_{an}$

and $a_{Ca\text{-}Ts}$, a_{en}, a_{an}, a_{fo} are the activities of Ca-Tschermak in clinopyroxene, enstatite in orthopyroxene, forsterite in olivine and anorthite in plagioclase.

Considering P as dependent variable, and assuming that ΔH, ΔV and ΔS are independent on pressure and temperature, the above relation can be recast as:

$$P = A + B\,\mathbf{T} + C\,T\,\ln\mathbf{K} \qquad (2)$$

where K is defined as above, and A, B, C are best considered as fit parameters for the barometer calibration rather than estimates of thermodynamic properties of the end-member equilibria, as no heat capacities and changes in volume as a function of P and T were included in our calculation.

The dependence of experimental values of lnK vs P/T and 1/T is shown in Figure 8. Errors in lnK have been derived by errors propagation of analytical uncertainties in the mineral chemistry of all phases involved. The lnK is strongly correlated with P/T. Although the range of temperature investigated is limited to the interval 1000-1150°C, Figure 8b also shows no significant dependence of lnK on temperature, further suggesting the robustness of the equilibrium (1) as a geobarometer.

In the following, we will derive the activity-models for mineral phases involved in equilibrium (1), we describe the fitting procedure and then discuss the calibration of the FACE geobarometer.

ACTIVITY-COMPOSITION RELATIONS

Plagioclase

Plagioclase solid solution has been considered as non ideal. The anorthite activity (a_{an}) has been calculated following the Darken's quadratic Formalism (DQF) model of Holland and Powell (1992). The same approach has been followed by McCarthy and Patiño Douce (1998) to calibrate the Silica – Ca-Tschermak - Anorthite (SCAn) geobarometer valid for SiO_2-saturated bulk compositions.

This model takes into account the structural changes related to the order/disorder transition from $C\bar{1}$ to $I\bar{1}$ structure in plagioclase and considers the two structures as separate simple solid solutions (Carpenter and McConnel, 1984). This approach is motivated for the calibration of the present data as plagioclase spans over a wide range of compositions that cross the transition at temperatures 1050-1150°C. The limit of the order-disorder transition $C\bar{1}$ to $I\bar{1}$ is calculated by the relation:

$$X_b = 0.12 + 0.00038\ T\ (K)$$

where X_b is the composition of plagioclase at the transition. Below the X_b limit, the activity of anorthite in plagioclase can be derived by assuming a $C\bar{1}$ structure characterized by a largely disordered distribution of Al and Si in tetrahedral that becomes short-range ordered as temperature decreases (Holland and Powell 1992). The molar fraction $X_{An,c}$ in the $C\bar{1}$ state is therefore calculated by the Al-avoidance model (Kerrick and Darken 1975) as:

$$X_{An,c} = ¼\ X_{An}(1+X_{An})^2$$

where $X_{An} = Ca/(Ca+Na)$.

Above the X_b limit, the molar fraction of anorthite in plagioclase is derived by assuming a $I\bar{1}$ structure characterized by a high degree of order and therefore the molar fraction of anorthite is given by:

$$X_{An,i} = X_{An}$$

The molar fractions defined above are then used to calculate the energy difference between the two structural states (I_{An}) as follow:

$$I_{An} = -RT \ln (X_{An,c}/X_{An}) - (W_c - W_i)(1-X_b)^2$$

where $W_C = 1070.0$ Jmol-1 , and $W_I = 9790.0$ Jmol-1 (Holland and Powell 1992).

Finally, the activity of anorthite in plagioclase ($a_{An,c}^{Pl}$) is calculated as follows:

$$a_{An,c}^{Pl} = X_{An,c} \exp (1/RT[W_c\ (1 - X_{An})^2 + I_{An}])$$

Clinopyroxene

Several activity models have been suggested for clinopyroxene (e.g. Herzberg, 1978; Wood and Banno, 1973). For the purpose of this study clinopyroxene is treated as an ideal three-site solid solution following Wood (1979). Mixing on all sites is considered independently according to a disordered model with random mixing and no local charge balance. As no oxygen buffering

technique has been adopted in none of the experiments used for calibration, no attempt to recalculate Fe^{3+} has been made; all Fe is considered as Fe^{2+}. Indeed Fe^{3+} content is expected to be negligible as the Pt-graphite assembly, together with pre-conditioning of the starting material at FMQ, maintain the oxygen fugacity at extremely reducing conditions, below the graphite-C-O vapour buffer.

The activity for Ca-Tschermak component is calculated as:

$$a_{Cats} = 4\, X_{Ca}\, X_{Al}{}^{M1}\, X_{Al}{}^{T}\, X_{Si}{}^{T}$$

Molar fractions have been determined adopting the procedure proposed by Carswell (1991) for chemically complex natural orthopyroxenes. This recalculation scheme enables reliable evaluation of Al content in the tetrahedral site, avoiding bias related to analytical uncertainty in Si determination. In particular, on a 6 oxygen basis, it follows:

$$Al^{IV} = (Al_{tot} + Cr + 2Ti - Na)/2$$
$$Al^{VI} = Al_{tot} - Al^{IV}$$
$$X_{Al}{}^{M1} = Al^{VI}$$
$$X_{Al}{}^{T} = Al^{IV}/(Si+Al^{IV})$$
$$X_{Si}{}^{T} = Si/(Si+Al^{IV})$$
$$X_{Ca}{}^{M2} = Ca$$

Olivine and orthopyroxene

Orthopyroxene solid solution has been treated as an ideal two-site solid solution with a random distribution of Fe and Mg in M1 and M2 (Wood and Banno 1973). As for clinopyroxene all Fe is treated as Fe^{2+}, and Al^{VI} is determined as $Al^{VI} = (Al+Cr+2Ti-Na)/2$ following Carswell (1991). The activity of enstatite in orthopyroxene is thus calculated as:

$$a_{en} = X_{Mg}{}^{M2}\, X_{Mg}{}^{M1}$$

where

$$X_{Mg}{}^{M2} = (Mg/(Ca+Mg+Fe+Na))_{M2}$$
$$X_{Mg}{}^{M1} = (Mg/(Fe+Al^{VI}+Ti+Cr+Mg))_{M1}$$

Olivine has been considered as an ideal two-site solid solution and activity of forsterite has been calculated as:

$$a_{fo} = X_{Mg}^2$$

where X_{Mg} = Mg/(Mg+Fe).

EMPIRICAL FIT: THE CALIBRATION OF THE FACE GEOBAROMETER

The calibration of the geobarometer requires to fit equation (2) to the dataset using a multiple linear-regression to solve for the parameters A, B, and C. This has been achieved using a least-squares method as a build-in function of the Mathematica software. In order to take into account error propagation of uncertainties in analytical determination of lnK, and uncertainties in experimental pressures (estimated to be around 0.3%) and temperature (± 20°C) a Monte Carlo approach has been coupled to regression analysis. Different sets of data have been therefore obtained by collecting 10000 randomly distributed values around the averages of lnK, P, and T within the standard deviation range. For each set of data the linear regression has been performed and the mean of all regressed parameters have been calculated together with standard deviations.

The complete dataset used for the regression is reported in Table 4. The least squares fit leads to the following calibration, where P is in kbar and T in kelvin:

$$P = 7.2\ (\pm 2.9) + 0.0078\ (\pm 0.0021)\ T + 0.0022\ (\pm 0.0001)\ T\ \ln K \qquad (3)$$

$$R^2 = 0.93$$

The standard error of estimate is 0.42 kbar. The error propagation of experimental P and T and lnK uncertainties performed by Monte Carlo approach results in an uncertainty of pressure of about ± 0.5 kbar.

Figure 9 shows the relation between experimental pressures and pressures calculated using equation 3. The relation close to 1:1 indicates that the model equation adequately explains the mineral chemistry variations as a function of P and T.

Residuals for each experimental point (i.e. the difference between calculated pressure and experimental pressure) are plotted vs. the two covariates T and lnK in Figure 10a,b. Errors are uncorrelated with T and lnK, demonstrating a good quality of the fit. No correlation with compositional variables is found. Importantly, no correlation exists between residuals and Na_2O/CaO in the bulk composition (Fig. 10c). These observations suggest that the barometer can be safely applied over a relatively wide range of bulk compositions in peridotites (see also Fig. 1).

If errors of fit parameters A, B and C are taken into account, greater propagated errors in predicted pressures are obtained, suggesting an accuracy that is better than 2.5 and 3 kbar. Such errors are of the same magnitude as estimated by Hodges and Crowley (1985) for other empirical barometers, and further reported by Kohn and Spear (1989).

In the Supplementary Material we provide a spreadsheet that enables to calculate the phase activities necessary to compute the lnK of the reaction (1), and thus obtain the equilibrium pressure by applying equation (3).

APPLICATION OF FACE BAROMETER TO NATURAL PERIDOTITES: TRACKING OF MANTLE EXHUMATION AT EXTENSIONAL SETTINGS

A fundamental requisite for a correct application of the geobarometric equation (3) is the accuracy in coupling mineral compositions and textural occurrence. In Borghini et al. (2011), we already discussed the applicability of experimental data to derive geobarometric estimates for natural peridotites. We showed that detailed microanalytical work and textural observations on plagioclase lherzolites from the External Liguride ophiolites (Northern Apennines) revealed systematic chemical zoning in texturally associated plagioclase and pyroxene neoblasts, documenting two major stages of equilibration within the plagioclase-facies stability field.

Here we apply the FACE geobarometer to the same plagioclase lherzolites studied by Borghini et al. (2011). We have estimated equilibrium pressure for three samples (ERS2-2, BG1, and BG6; Borghini et al. 2011), by distinguishing neoblasts cores and rims (stage1 and stage2, respectively). We derived the equilibrium temperature applying the two-pyroxene thermometer of Taylor (1998) to clinopyroxene and orthopyroxene pair from single neoblastic assemblages. The thermometer of Taylor (1998) has been reported to be more robust as compared, for example, with the two-pyroxene thermometer of Brey and Köhler (1990), especially for high-Na clinopyroxene compositions (Nimis and Grütter, 2010). The results are shown in Figure 11, where P-T estimates (S1) and (S2) refer to stage1 and stage2 defined above. Equilibrium pressures are comprised between 6.3 and 7.0 kbar for neoblastic cores (stage1) at temperature 840-900°C, and between 4.3-4.8 kbar for neoblastic rims (stage2) at temperature 800-850°C (Fig. 11).

Figure 11 also reports for comparison the pressure estimates previously derived by Borghini et al. (2011) on the same plagioclase-clinopyroxene pairs, using the anorthite isopleths experimentally calibrated only for FLZ. Borghini et al. 2011, estimating temperatures slightly higher as a result of averaged values from different geothermometers reported pressure values of stage1 and stage2 of 7 and 3 kbar, respectively. The approximation introduced by using the simplified single-plagioclase empirical equation of Borghini et al. (2011) is therefore to underestimate the pressure at low

temperature (Fig. 11). The application of the FACE geobarometer confirms the decompressional evolution previously envisaged for this External Liguride mantle sector. Results obtained using Taylor (1998) geothermometer have been compared with pressure defined by using the Ca-in-opx geothermometer of Brey and Köhler (1990) resulting in a negligible change in pressure (Suppl. Figure 2s). As suggested by the isopleths for constant lnK calculated using equation (3), temperature has a minor effect on computed pressure (Fig. 11). An uncertainty of 100°C in temperature estimate results in a maximum pressure deviation of about 0.3 kbar in a pressure range between 2 and 3 kbar, where the isopleths slope is higher.

The FACE geobarometer has been also applied to plagioclase peridotites from Lanzo (Western Alps) studied by Kaczmarek and Müntener (2008). These authors investigated several plagioclase peridotite samples, and provided a very detailed dataset combining field and microstructural observations with exhaustive mineral chemistry. These plagioclase peridotites experienced melt migration and high-temperature deformation juxtaposed in time and space, within a kilometer-scale shear zone. Progressive deformation is testified by development of textures evolving from porphyroclastic to fine-grained porphyroclastic, to proto-mylonitic, to mylonitic. Grain-size reduction and deformation have been enhanced by melt infiltration and melt-rock reaction, as supported by variably refertilized bulk composition in the most deformed samples (Kaczmarek and Müntener 2010). Application of our geobarometer to five peridotite samples (L04, L112, La02-5, L09 and L241) provides equilibrium pressures in the range 2.4-4.4 kbar (Figure 11). Remarkably, there is a correlation between pressure and grain-size reduction, i.e. increasing degree of deformation, with lower pressure estimates yielded by peridotites with mylonitic textures (P-M and M; Figure 11). This evidence well supports the inference by Kaczmareck and Müntener (2008) that deformation and melt focusing in the extensional shear zone accompanied progressive exhumation at shallow lithospheric environments of this Lanzo mantle sector.

Other interesting case studies are represented by plagioclase peridotites exposed along the Hidaka metamorphic belt. The most relevant are peridotite complexes from the Horoman (Ozawa and Takahashi 1995; Takazawa et al. 1996), Uenzaru (Furusho and Kanagawa 1999), and Nikanbetsu (Takahashi 2001) belts. Major element compositions of neoblasts from plagioclase-bearing assemblages were reported by Takahashi (2001), for the Nikanbetsu peridotite. Application of our geobarometer yields pressures from 7.2 kbar in neoblast cores, to 5.4 kbar in neoblast rims (Fig. 11), consistent with the decompressional evolution inferred for this peridotite complex (Takahashi, 2001). Similar results were obtained by Ozawa and Takahashi (1995), who for the first time discussed the presence of reverse anorthite zoning in plagioclase as a result of the progressive subsolidus exhumation. They derived P-T decompression trajectory of Upper and Lower Horoman

mantle sectors as inferred by An-isopleths in plagioclase and Al-isopleths in coexisting orthopyroxene determined by Gasparik (1987) in NCMAS. Furusho and Kanagawa (1999) also proposed a similar evolution for mylonitic plagioclase peridotites from the Uenzaru complex. Unfortunately, the lack of texturally controlled chemical analysis on plagioclase-bearing neoblasts prevents the application of the FACE geobarometer to these peridotites.

CONCLUDING REMARKS

Results of experiments performed on a Na_2O-enriched lherzolite (HNa-FLZ) at plagioclase-facies conditions have been combined to previous investigations on fertile (FLZ) and depleted (DLZ) lherzolite, in order to build a robust experimental mineral chemistry dataset, covering a large range of peridotite bulk compositions (Na_2O/CaO = 0.08 – 0.13; X_{Cr} = 0.07 – 0.10), in the subsolidus mantle P-T range 2.5-10 kbar, 1000-1150°C. This dataset has been used to calibrate empirically a geobarometer based on the pressure-sensitive equilibrium Forsterite + Anorthite = CaTschermak + Enstatite (FACE), providing an equation to derive pressure as a function of lnK of the reaction and temperature.

Application of the FACE geobarometer requires a careful microstructural observation combined to detailed analytical work on texturally associated neoblasts from plagioclase-bearing mineral assemblages in mantle peridotites. When applied to case studies having the required microstructural and mineral chemistry background, the proposed geobarometer appears to be a valuable tool to trace the exhumation of the lithospheric mantle in extensional environments.

Our experimental data, integrated with previous experimental studies, also allowed to better define the P-T field of plagioclase-facies stability for mantle lherzolites. At near-solidus temperature conditions, the spinel- to plagioclase-facies transition in variably depleted lherzolites is approximately located between 7-10 kbar, the plagioclase-out boundary being mostly influenced by Na_2O/CaO and X_{Cr} ratios in the bulk rock.

AKNOWLEDGMENTS

The authors wish to thank A. Risplendente for the precious assistance at the electron microprobe. The authors are thankful to C. Herzberg and P. Nimis for their reviews, and to O. Müntener for his valuable work as editor.

REFERENCES

Beslier M-O, Ask M, Boillot G (1993) Ocean-continent boundary in the Iberia Abyssal Plain from multichannel seismic data. Tectonophysics 218:383–393

Bodinier JL, Dupuy C, Dostal J (1988) Geochemistry and petrogenesis of Eastern Pyrenean peridotites. Geochimica et Cosmochimica Acta 52:2893–2907

Bodinier JL, Garrido CJ, Chanefo I, Bruguier O, Gervilla F (2008) Origin of pyroxenite–peridotite veined mantle by refertilization reactions: Evidence from the Ronda peridotite (Southern Spain). J Petrol 49:999–1025

Borghini G, Rampone E, Crispini L, De Ferrari R, Godard M (2007) Origin and emplacement of ultramafic-mafic intrusions in the Erro-Tobbio mantle peridotite (Ligurian Alps, Italy). Lithos 94:210–229

Borghini G, Fumagalli P, Rampone E (2010) The stability of plagioclase in the upper mantle: subsolidus experiments on fertile and depleted lherzolite. J Petrol 51:229–254

Borghini G, Fumagalli P, Rampone E (2011) The geobarometric significance of plagioclase in mantle peridotites: A link between nature and experiments. Lithos 126:42–53

Bonadiman C, Beccaluva L, Coltorti M, Siena F (2005) Kimberlite-like metasomatism and 'garnet signature' in spinel–peridotite xenoliths from Sal, Cape Verde archipelago: relics of a subcontinental mantle domain within the Atlantic oceanic lithosphere? J Petrol 46:2465–2493

Bonatti E, Ottonello G, Hamlyn PR (1986) Peridotites from the island of Zabargad (St. John), Red Sea: petrology and geochemistry. J Geophys Res 91:599–631

Brey GP, Köhler T (1990) Geothermobarometry in four-phase lherzolites II. New thermobarometers, and practical assessment of existing thermobarometers. J Petrol 31:1353–1378

Brunelli D, Seyler M (2010) Asthenospheric percolation of alkaline melts beneath the St. Paul region (Central Atlantic Ocean). Earth Planet Sci Lett 289:393–405

Cannat M, Seyler M. (1995) Transform tectonics, metamorphic plagioclase and amphibolitization in ultramafic rocks of the Vema transform fault (Atlantic Ocean). Earth Planet Sci Lett 133:283–298

Carpenter MA, McConnell JDC (1984) Experimental delineation of the C1=I1 transition in intermediate plagioclase feldspars. American Mineralogist 69:112–121

Chalot-Prat F, Falloon TJ, Green DH, Hibberson WO (2010) An experimental study of liquid compositions in equilibrium with plagioclase + spinel lherzolite at low pressure (0.75 GPa). J Petrol 51:2349–2376

Chalot-Prat F, Falloon TJ, Green DH, Hibberson WO (2013) Melting of plagioclase + spinel lherzolite at low pressure (0.5 GPa): An experimental approach to the evolution of basaltic melt during mantle refertilization at shallow depths. Lithos 172–173:61–80

Chazot G, Charpentier S, Kornprobst J, Vannucci R, Luais B (2005) Lithospheric mantle evolution during continental break-up: the west Iberia non-volcanic passive margin. J Petrol 46:2527–2568

Dick HJB, Bullen TD (1984) Chromian spinel as a petrogenetic indicator in abyssal and alpine-type peridotites and spatially associated lavas. Contrib Mineral Petrol 86:54–76

Dick HJB, Lissemberg CJ, Warren J (2010) Mantle melting, melt transport, and delivery beneath a slow-spreading ridge: the paleo-MAR from 23°15'N to 23°45'N. J Petrol 51:425-467

Dick HJB (1989) Abyssal peridotite, very slow spreading ridges and oceanic ridge magmatism. In: Saunders, A. D. Morris M.J. (Eds.), Magmatism in the Ocean Basins. Spec Publ Geol Soc London 42:71–105

Falloon TJ, Green DH, O'Neill HSC, Hibberson WO (1997) Experimental tests of low degree peridotite partial melt compositions, implications for the nature of anhydrous near-solidus peridotite melts at 1 GPa. Earth Planet Sci Lett 152:149–162

Frey FA, Shimizu N, Leinbach A, Obata M, Takazawa E (1991) Compositional variations within the Lower Layered Zone of the Horoman peridotite, Hokkaido, Japan: Constraints on models for melt-solid segregation. In Orogenic Lherzolite and Mantle Processes (ed. M. A. Menzies et al.); J Petrol 211–227.

Fumagalli P, Klemme S (2015) Mineralogy of the Earth: Phase Transitions and Mineralogy of the Upper Mantle. In: Gerald Schubert (editor-in-chief) Treatise on Geophysics, 2nd edition, Oxford: Elsevier, vol. 2:7–31

Furusho M, Kanagawa K, (1999) Transformation-induced strain localization in a lherzolite mylonite from the Hidaka metamorphic belt of central Hokkaido, Japan. Tectonophysics 313:411–432

Gasparik T (1984) Two-pyroxene thermobarometry with new experimental data in the system CaO-MgO-Al_2O_3-SiO_2. Contrib Mineral Petrol 87:87–97

Gasparik T (1985) Experimental study of subsolidus phase relations and mixing properties of pyroxene and plagioclase in the system Na_2O-CaO-Al_2O_3-SiO_2. Contrib Mineral Petrol 89:346–357

Gasparik T (1987) Orthopyroxene thermobarometry in simple and complex systems. Contrib Mineral Petrol 96:357–370

Green DH (1964) The petrogenesis of the high-temperature peridotite intrusion in the Lizard Area, Cornwall. J Petrol 5:134–188

Green DH, Hibberson W (1970) The instability of plagioclase in peridotite at high pressure. Lithos 3:209–221

Green DH, Hibberson WO, Jaques AL (1979) Petrogenesis of mid ocean ridge basalt. In: McElhinney, M. W. (ed.) The Earth: its Origin, Structure and Evolution. London: Academic Press, 265–299

Green DH, Falloon TJ (1998) Pyrolite: A Ringwood concept and its current expression. In: Jackson, I. (ed) The Earth's Mantle. Cambridge: Cambridge University Press, pp. 311–378

Hamilton DL, Henderson CMB (1968) The preparation of silicate compositions by a gelling method. Mineral Mag 36:832–838.

Hamlyn PR, Bonatti E (1980) Petrology of mantle-derived ultramafic from the Owen fracture zone, northwest Indian Ocean: implications for the nature of the oceanic upper mantle. Earth Planet Sci Lett 48:65–79

Herzberg CT (1978) Pyroxene geothermometry and geobarometry: experimental and thermodynamic evaluation of some subsolidus phase relations involving pyroxenes in the system CaO-MgO-Al_2O_3-SiO_2. Geochimica et Cosmochimica Acta 42:945–957

Hidas K, Garrido C, Tommasi A, Padron-Navarta JA, Thielmann M, Konc Z, Frets E, Marchesi C (2013) Strain localization in pyroxenite by reaction-enhanced softening in the shallow subcontinental lithospheric mantle. J Petrol 54:1997–2031

Hodges HV, Crowley PD (1985) Error estimation and empirical geothermobarometry for politic systems. Am Mineral 70:702–709

Holland T, Powell R (1992) Plagioclase feldspars: activity-composition relations based upon Darken's quadratic formalism and Landau theory. American Mineralogist 77:53–61

Ionov DA, O'Reilly SY, Ashchepkov V (1995) Feldspar-bearing lherzolite xenoliths in alkali basalts from Hamar–Daban Baikal region, Russia. Contrib Mineral Petrol 122:174–190

Kaczmarek MA, Müntener O (2008) Juxtaposition of melt impregnation and high-temperature shear zones in the upper mantle; field and petrological constraints from the Lanzo peridotite (Northern Italy). J Petrol 49:2187–2220

Kaczmarek MA, Müntener O (2010) The variability of peridotite composition across a mantle shear zone (Lanzo massif, Italy): interplay of melt focusing and deformation. Contrib Mineral Petrol 160:663–679

Kelemen PB, Kikawa E, Miller DJ (2007) Leg 209 summary: processes in a 20-km-thick conductive boundary layer beneath the Mid-Atlantic Ridge, 14_-16_N. In Proceedings of the ODP, science results 209 (eds. P. B. Kelemen, E. Kikawa and D. J. Miller). Ocean Drilling Program, College Station, TX, pp. 1–33

Kerrick DM, Darken LS (1975) Statistical thermodynamic models for ideal oxide and silicate solutions, with applications to plagioclase. Geochimica et Cosmochimica Acta 39:1431–1442

Kinzler RJ (1997) Melting of mantle peridotite at pressures approaching the spinel to garnet transition: application to mid-ocean ridge basalt petrogenesis. J Geophys Res 102:853–874

Klemme S (2004) The influence of Cr on the garnet-spinel transition in the Eatrh's mantle: experiments in the system MgO-Cr_2O_3-SiO_2 and thermodynamic modelling. Lithos 77:639–646

Kohn MJ and Spear FS (1989) Empirical calibration of geobarometers for the assemblage garnet + hornblende + plagioclase + quartz. Am Mineral 74:77–84

Kornprobst J, Tabit A (1988) Plagioclase-Bearing ultramafic tectonites from the Galicia margin (Leg 103, Site 637): comparison of their origin and evolution with low pressure ultramafic bodies in western Europe. Proceeding into Ocean Drilling Project Science Research 103:253–263

Kushiro I, Yoder HS (1966) Anorthite-forsterite and anorthite-enstatite reactions and their bearing on the basalt-eclogite transformation. J Petrol 7:337–362

Leake BE (1997) Nomenclature of amphiboles: Report of the Subcommittee on Amphiboles of the International Mineralogical Association, Commission on New Minerals and Mineral Names. American Mineralogists 82:1019–1037

Le Roux V, Bodinier JL, Tommasi A, Alard O, Dautria JM, Vauchez A, Riches AJV (2007) The lherz spinel lherzolite: refertilized rather than pristine mantle. Earth Planet Sci Lett 259:599–612

Martin AP, Cooper AF, Price RC (2014a) Increased mantle heat flow with on-going rifting of the West Antarctic rift system inferred from characterisation of plagioclase peridotite in the shallow Antarctic mantle. Lithos 190–191:173–190

Martin AP, Price RC, Cooper AF (2014b) Constraints on the composition, source and petrogenesis of plagioclase-bearing mantle peridotite. Earth-science Reviews 138:89–101

Manatschal G (2004) New models for evolution of magma-poor rifted margins based on a review of data and concepts from West Iberia and the Alps. International Journal of Earth Sciences 93:432–466

Manatschal G, Müntener O (2009) A type sequence across an ancient magma-poor ocean–continent transition: the example of the western Alpine Tethys ophiolites. Tectonophysics 473:4–19

McCarthy TC, Patino-Douce E (1998) Empirical calibration of the silica-Ca-tschermak's-anorthite (SCAn) geobarometer. J Metamorphic Geol 16:675–686

Michael PJ, Langmuir CH, Dick HJB, Snow JE, Goldstein SL, Graham DW, Lehnert K, Kurras G, Jokat W, Muhe R, Edmonds HN (2003) Magmatic and amagmatic seafloor generation at the ultraslow-spreading Gakkel ridge, Arctic Ocean. Nature 423:956–961

Montanini A, Tribuzio R, Anczkiewicz R (2006) Exhumation history of a garnet pyroxenite-bearing mantle section from a continent-ocean transition (Northern Apennine ophiolites, Italy). J Petrol 47:1943–1971

Müntener O, Manatschal G (2006) High degrees of melt extraction recorded by spinel harzburgite of the Newfoundland margin: The role of inheritance and consequences for the evolution of the southern North Atlantic. Earth Planet Sci Lett 252:437–452

Müntener O, Pettke T, Desmours L, Meier M, Schaltegger U (2004) Refertilization of mantle peridotite in embryonic ocean basins: trace element and Nd-isotope evidence and implications for crust-mantle relationships. Earth Planet Sci Lett 221:293–308

Müntener O, Manatschal G, Desmours L, Pettke T (2010) Plagioclase peridotites in ocean-continent transitions: refertilized mantle domains generated by melt stagnation in the shallow mantle lithosphere. J Petrol 51:255–294

Newman J, Lamb WM, Drury MR, Vissers RLM (1999) Deformation processes in a peridotite shear zone: reaction-softening by an H_2O-deficient, continuous net transfer reaction. Tectonophysics 303:193–222

Niida K, Green DH (1999) Stability and chemical composition of pargasitic amphibole in MORB pyrolite under upper mantle conditions. Contrib Mineral Petrol 135:18–40

Nimis P, Grütter H (2010) Internally consistent geothermometers for garnet peridotites and pyroxenites. Contrib Mineral Petrol 159:411–427

Niu YL (2004) Bulk-rock major and trace element compositions of abyssal peridotites: implications for mantle melting, melt extraction and post-melting processes beneath mid-ocean ridges. J Petrol 45:2423–2458

Obata M (1976) The solubility of Al_2O_3 in orthopyroxenes in spinel and plagioclase peridotites and spinel pyroxenite. American Mineralogists 61:804–816

Obata M (1980) The Ronda peridotite: garnet-spine1 and plagioclase-lherzolite and the P-T trajectories of a high-temperature mantle intrusion. J Petrol 21:533–572

Ozawa K, Takahashi N (1995) P–T history of a mantle diapir: the Horoman peridotite complex, Hokkaido, northern Japan. Contrib Mineral Petrol 120:223–248

Piccardo, G.B., Messiga, B., Vannucci, R., 1988. The Zabargad peridotite–pyroxenite association: petrological constraints on its evolution. Tectonophysics 150, 135–162.

Piccardo GB, Müntener O, Zanetti A, Pettke T (2004) Ophiolitic peridotites of the Alpine-Apennine system: mantle processes and geodynamic relevance. International Geology Review 46:1119–1159

Piccardo GB, Vissers RLM (2007) The pre-oceanic evolution of the Erro-Tobbio peridotite (Voltri Massif, Ligurian Alps, Italy). Journal of Geodynamics 43:417–449

Piccardo GB, Zanetti A, Poggi E, Spagnolo G, Müntener O (2007) Melt/peridotite interaction in the Lanzo South peridotite: field, textural and geochemical evidence. Lithos 94:181–209

Presnall DC, Dixon JR, O'Donnell TH, Dixon SA (1979) Generation of mid-ocean ridge tholeiites. J Petrol 20:3–35

Rampone E, Piccardo GB, Vannucci R, Bottazzi P, Ottolini L (1993) Subsolidus reactions monitored by trace element partitioning: the spinel- to plagioclasi-facies transition in mantle peridotites. Contrib Mineral Petrol 115:1–17

Rampone E, Hofmann AW, Piccardo GB, Vannucci R, Bottazzi P, Ottolini L (1995) Petrology, mineral and isotope geochemistry of the External Liguride peridotites (Northern Apennines, Italy). J Petrol 123:61–76.

Rampone E, Hofmann AW, Piccardo GB, Vannucci R, Bottazzi P, Ottolini L (1996) Trace element and isotope geochemistry of depleted peridotites from an N-MORB type ophiolite (Internal Liguride, N.Italy). Contrib Mineral Petrol 123:61–76

Rampone E, Piccardo GB, Vannucci R, Bottazzi P (1997) Chemistry and origin of trapped melts in ophiolitic peridotites. Geochimica et Cosmochimica Acta 61:4557–4569

Rampone E, Romairone A, Abouchami W, Piccardo GB, Hofmann W (2005) Chronology, petrology and isotope geochemistr of the Erro-Tobbio peridotites (Ligurian Alps, Italy): records of late Palaeozoic lithospheric extension. J Petrol 46:799–827

Rampone E, Piccardo GB, Hofmann AW (2008) Multi-stage melt-rock interaction in the Mt. Maggiore (Corsica, France) ophiolitic peridotites: microstructural and geochemical records. Contrib Mineral Petrol 156:453–475

Sano S, Kimura JI (2007) Clinopyroxene REE geochemistry of the Red Hills peridotite, New Zealand: interpretation of magmatic processes in the upper mantle and in the Moho transition zone. J Petrol 48:113–139

Secchiari A, Montanini A, Bosch D, Macera P, Cluzel D (2016) Melt Extraction and enrichment processes in the New Caledonia lherzolites: Evidence from geochemical and Sr-Nd isotope data. Lithos 260:28–43

Sinigoi S, Comin-Chiaramonti P, Alberti AA (1980) Phase relations in the partial melting of the Baldissero spinel-lherzolite (Ivrea–Verbano Zone, Western Alps, Italy). Contrib Mineral Petrol 75:111–121

Takahashi N (2001) Origin of plagioclase lherzolites from Nikanbetsu peridotite complex, Hokkaido, Northern Japan: implications for incipient melt migration and segregation in the partially molten upper mantle. J Petrol 42:39–54

Takazawa E, Frey F, Shimizu N, Obata M (1996) Evolution of the Horoman peridotite (Hokkaido, Japan): implications from pyroxene compositions. Chemical Geology 134:3–26

Takazawa E, Frey FA, Shimizu N, Obata M (2000) Bulk rock compositional variations in an upper mantle peridotite (Horoman, Hokkaido, Japan): are they consistent with a partial melting process? Geochimica et Cosmochimimica Acta 64:695–716

Taylor WR (1998) An experimental test of some geothermometer and geobarometer formulation for upper mantle peridotites with application to the thermobarometry of fertile lherzolite and garnet websterite. N Jb Min Abh 172:381–408

Tamura A, Arai S, Ishimaru S, Andal ES (2008) Petrology and geochemistry of peridotites from IODP Site U1309 at Atlantis Massif, MAR 30°N: micro- and macro-scale melt penetrations into peridotites. Contrib Mineral Petrol 155:491–509

Tartarotti P, Susini S, Nimis P, Ottolini L (2002) Melt migration in the upper mantle along the Romanche fracture zone (Equatorial Atlantic). Lithos 63:125–149

Ulmer P, Luth RW (1991) The graphite fluid equilibrium in P, T, fO2 space: an experimental determination to 30 kbar and 1600°C. Contrib Mineral Petrol 106:265–272

Van der Wal D, Vissers RLM (1996). Structural petrology of the Ronda peridotite, SW Spain: deformation history. J Petrol 37:23–43

Voshage H, Sinigoi S, Mazzucchelli M, Demarchi G, Rivalenti G, Hofmann AW (1988) Isotopic constraints on the origin of ultramafic and mafic dikes in the Balmuccia peridotite (Ivrea Zone). Contrib Mineral Petrol 100:261–267

Warren JM, Shimizu N (2010) Cryptic variations in abyssal peridotite compositions: evidence for shallow-level melt infiltration in the oceanic lithosphere. J Petrol 51:395–423

Warren JM (2016) Global variations in abyssal peridotite compositions. Lithos 248–251:193–219

Walter MJ, Presnall DC (1994) Melting behaviour of simplified lherzolite in the system CaO-MgO-Al_2O_3-SiO_2-Na_2O from 7 to 35 kbar. J Petrol 35:329–359

Walter MJ (1998) Melting of garnet peridotite and the origin of komatiite and depleted lithosphere. J Petrol 39:29–60

Wood BJ (1979) Activity–composition relationships in Ca (Mg, Fe) Si_2O_6–$CaAl_2SiO_6$ clinopyroxene solid solutions. American Journal of Science 279:854–875

Wood BJ, Banno, S (1973) Garnet-orthopyroxene and orthopyroxene-clinopyroxene relationships in simple and complex systems. Contrib Mineral Petrol 42:109–124

FIGURE CAPTIONS

Figure 1 Na_2O/CaO vs X_{Cr} = Cr/(Cr+Al) diagram showing the composition of starting materials used in this and previous experimental studies. FLZ: Fertile Lherzolite (this study, Borghini et al. 2010, 2011); DLZ: Depleted Lherzolite (this study, Borghini et al. 2010); HNa-FLZ: High-Na Fertile Lherzolite (HNa-FLZ, this study), TQ: Tinaquillo Lherzolite (Green 1963); MPY: MORB Pyrolite (Green et al. 1979); HPY: Hawaiian Pyrolite (Green et al. 1979). Experimental starting materials are compared with the compositions of ophiolitic, orogenic and oceanic peridotites (Sinigoi 1980; Bodinier et al. 1988, 2008; Piccardo et al. 1988; Frey et al. 1991; Van der Wal and Vissers 1996; Voshage et al. 1998; Rampone et al. 1995; 1996, 2005, 2008; Takazawa et al. 2000; Niu 2004; Sano and Kimura 2007; Le Roux et al. 2007; Kaczmarek and Müntener 2010), and mantle xenoliths (Ionov et al. 1995; Bonadiman et al. 2005; Martin et al. 2014a).

Figure 2 Run conditions of experiments performed in this study. The dashed line locates the transition from plagioclase-bearing assemblages to plagioclase-free phase assemblages in the Na-rich bulk composition (High-Na Fertile Lherzolite, HNa-FLZ).

Figure 3 Representative textures in plagioclase bearing experiments. (a) Back-Scattered-Electron (BSE) image of run at 7 kbar, 1150°C in composition FLZ; (b) BSE image of run at 6 kbar, 1100°C in composition HNa-FLZ; (c) BSE image of run at 8 kbar, 1100°C in HNa-FLZ bulk composition.

Figure 4 Variation of Ca/(Ca+Na) in alkali-bearing phases as a function of pressure for the three bulk compositions investigated. Abbreviations are cpx: clinopyroxene, pl: plagioclase; amp: amphibole. Grey symbols refer to previous experimental results in Borghini et al. (2010, 2011).

Figure 5 Variations of Al content in (a) clinopyroxene and (b) orthopyroxene as a function of pressure. Coloured symbols are for the present study, grey symbols for previous experiments reported in Borghini et al. (2010; 2011).

Figure 6 Location in the P-T diagram of the plagioclase-out boundary and solidus curves for bulk compositions investigated in this work as compared with data from previous experimental studies (MPY: MORB Pyrolite, Niida and Green 1999; HPY: Hawaiian Pyrolite, Green and Falloon 1998, LherzA: Lherzolite A, Presnall et al. 1979). The CIPW normative Albite/Diopside (Ab/Di_{CIPW}) ratio and the X_{Cr} ratio are reported, for each plagioclase-out boundary, in the corresponding empty circle.

Figure 7 X_{an} (Ca/(Ca+Na) in plagioclase vs. X_{Al}^{M1} in clinopyroxene showing the correlation with pressure. Available data from previous subsolidus and melting experimental studies are plotted as uncoloured symbols. See text for details.

Figure 8 Variation of equilibrium constant for the equilibrium (1) vs P/T (a) and 1/T (b).

Figure 9 Experimental pressure vs pressure calculated using equation (3). Horizontal error bars are defined by the accuracy in experimental pressure ± 3%. Vertical error bars have been determined by Monte Carlo simulation for each point of the calibration dataset (see text for details).

Figure 10 Residuals (experimental pressure - calculated pressure) vs lnK (a), T (b) and Na_2O/CaO (c).

Figure 11 Estimates of P-T equilibrium conditions for plagioclase-bearing assemblages. The decompressional evolution of Suvero Peridotite (External Liguride, Northern Apennine, Italy; Borghini et al. 2011) is traced by core-rim chemical variations in plagioclase-bearing neoblasts (the green symbols; see text for further details). Grey symbols are previous estimates based on anorthite in plagioclase isopleths (Borghini et al. 2011). For the Lanzo peridotites (Kaczamarek and Müntener 2008) textural features are also indicated as porphyroclastic (P), porphyroclastic fined grained (PFG), proto-mylonitic (PM) and mylonitic (M). Squares are pressure estimates using mineral composition of cores and rims from neoblasts from plagioclase-bearing assemblage in Nikanbetsu peridotites, Hokkaido, Northern Japan (Takahashi 2001). Blue lines are lnK isopleths calculated using equation (3); numbers refer to lnK values. Temperatures have been estimated with Taylor (1998) two-pyroxenes geothermometer (1990). Error bars for pressure have been derived by Monte Carlo simulation (see text for details).

Figure1

Click here to download Figure figure1.pdf

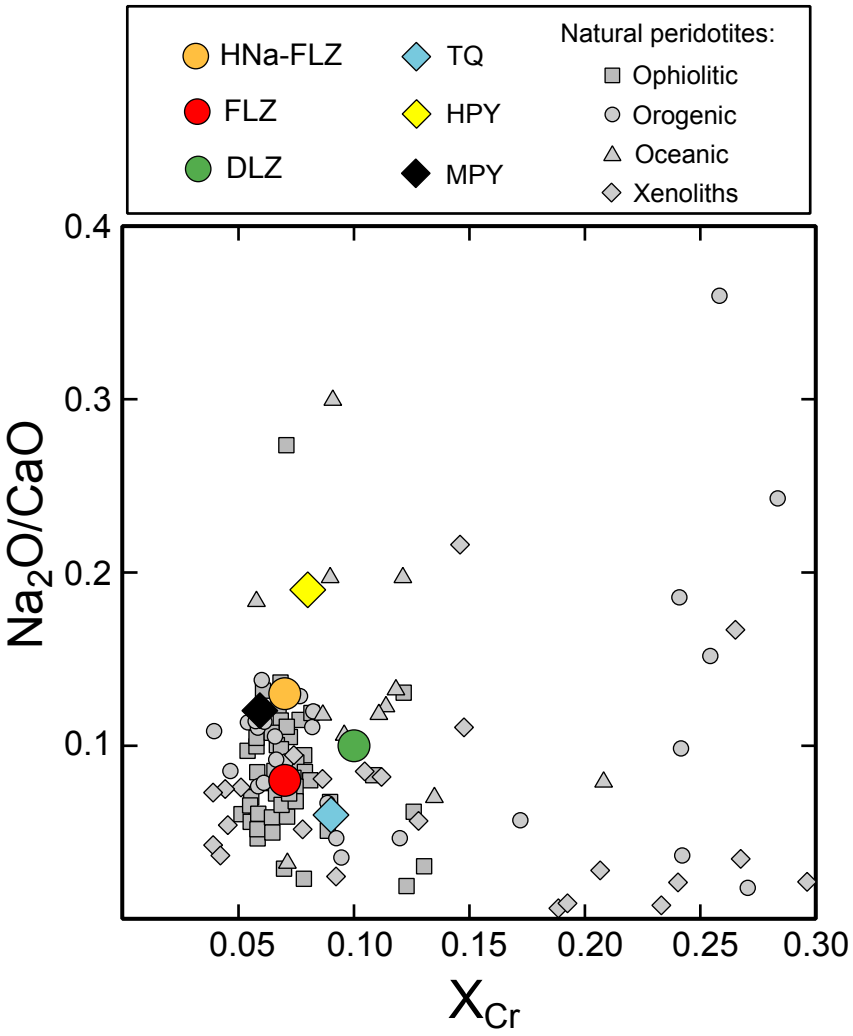

Figure2

Click here to download Figure figure2.pdf

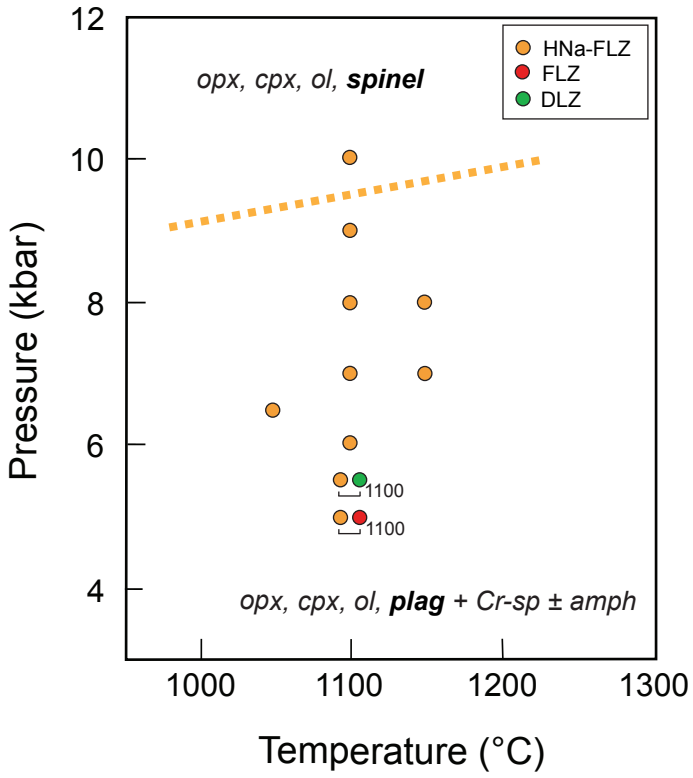

Figure3

Click here to download Figure figure3.pdf

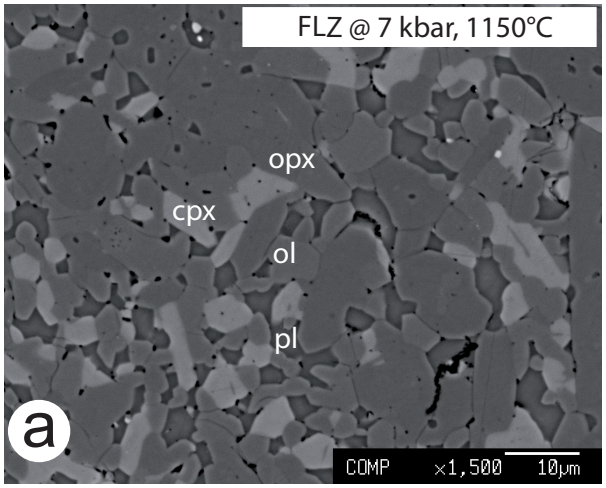

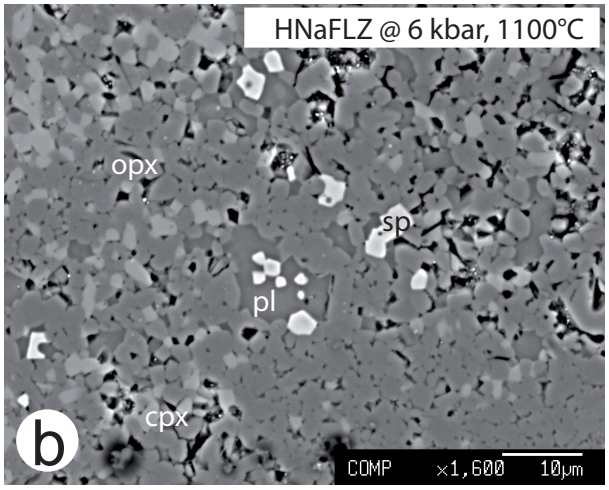

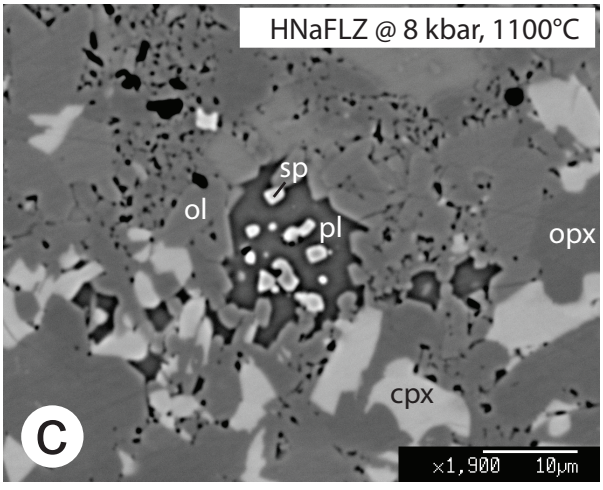

Figure4

Click here to download Figure figure4.pdf

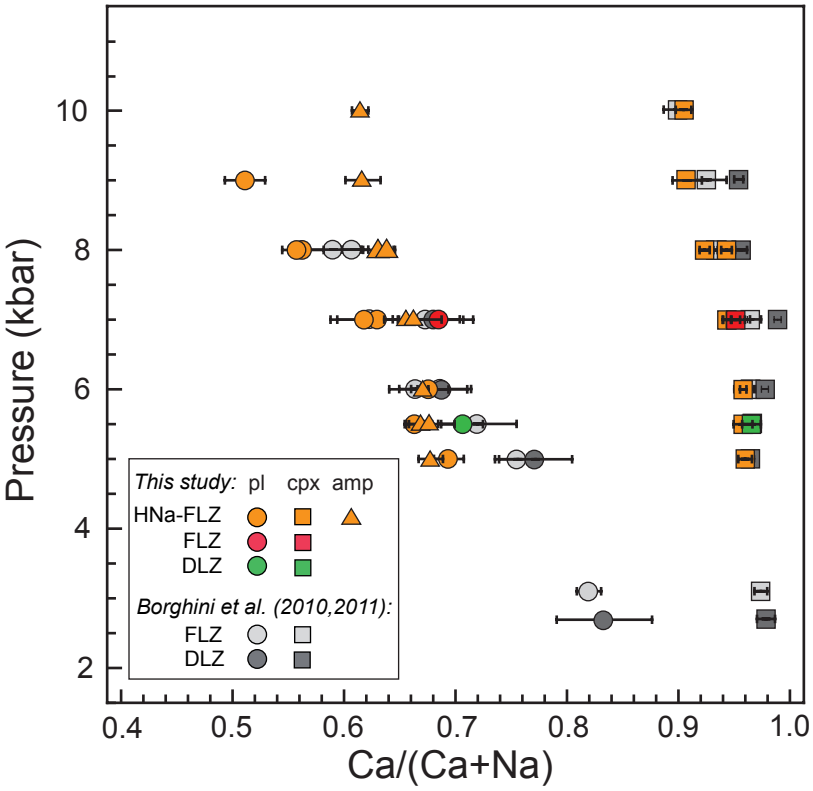

Figure5

Click here to download Figure figure5.pdf

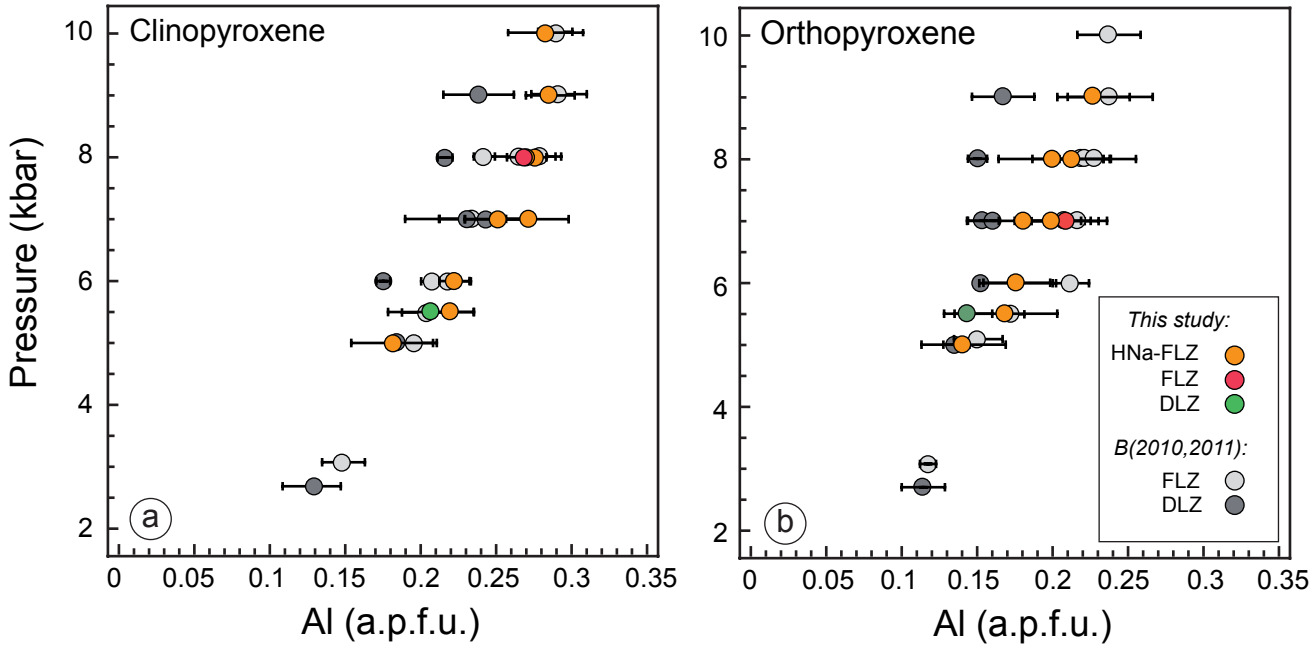

Figure6

Click here to download Figure figure6_ex7_rev.pdf

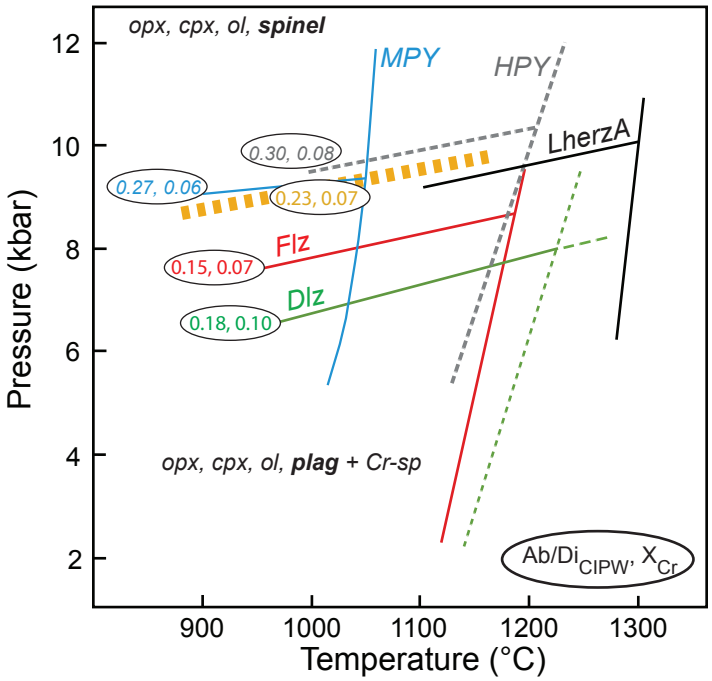

Figure7

Click here to download Figure figure7_ex6_rev.pdf

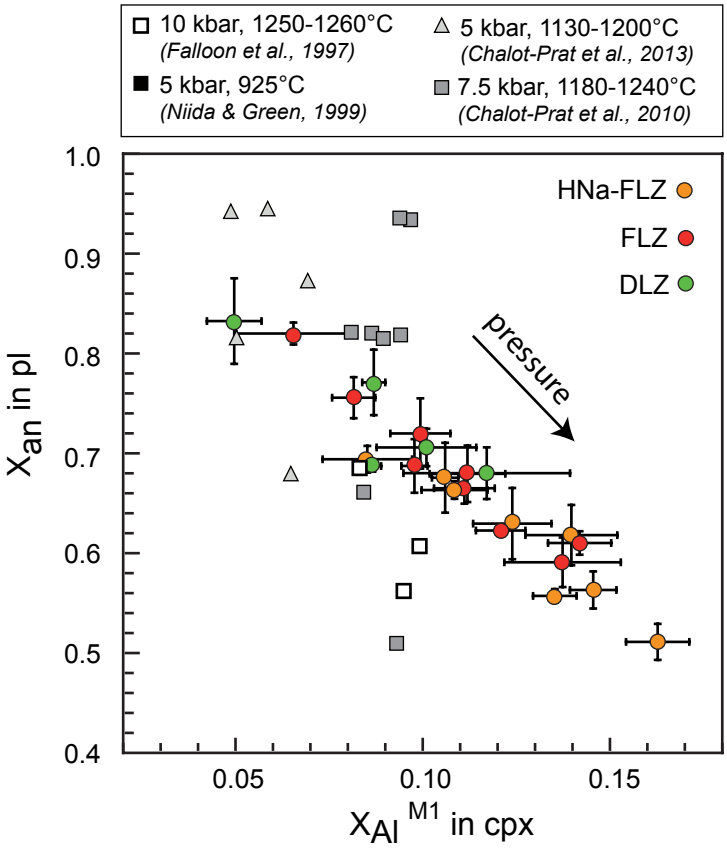

Figure8

Click here to download Figure figure8_rev.pdf

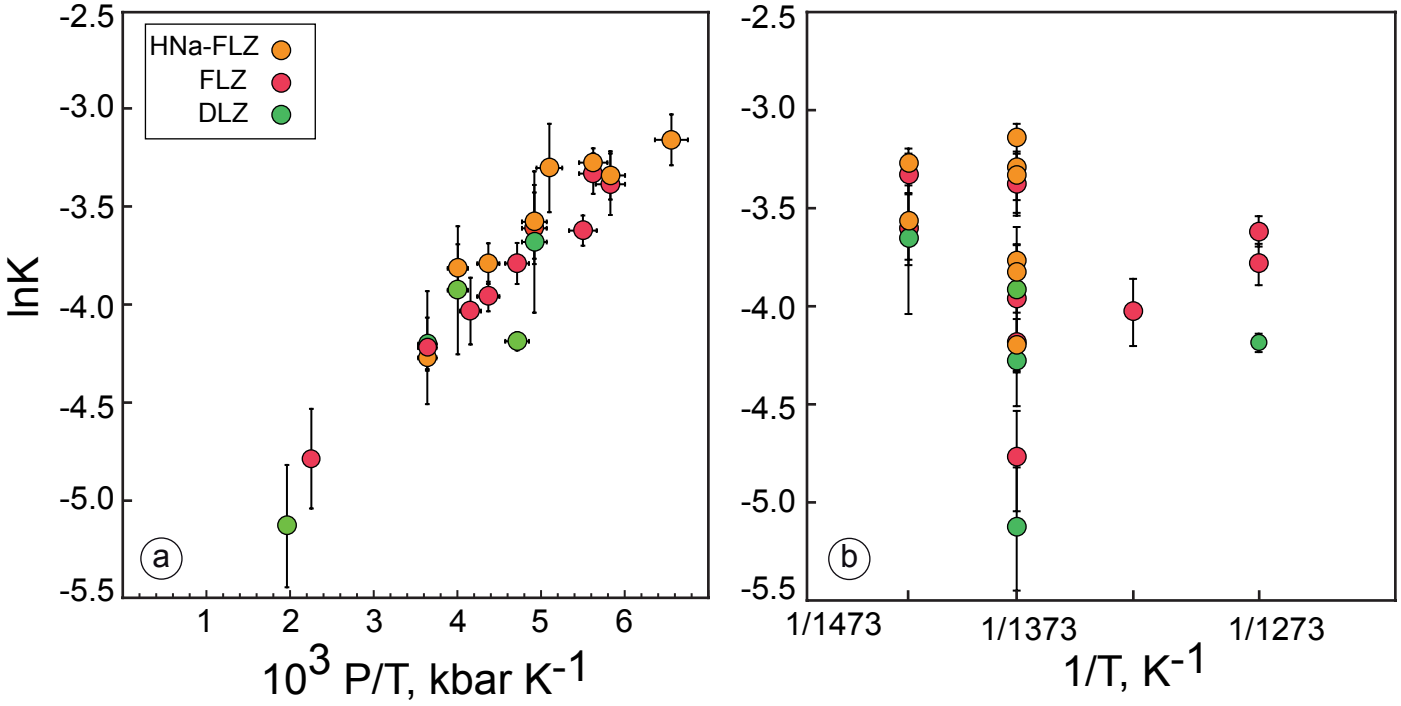

Figure9

Click here to download Figure figure9_rev.pdf

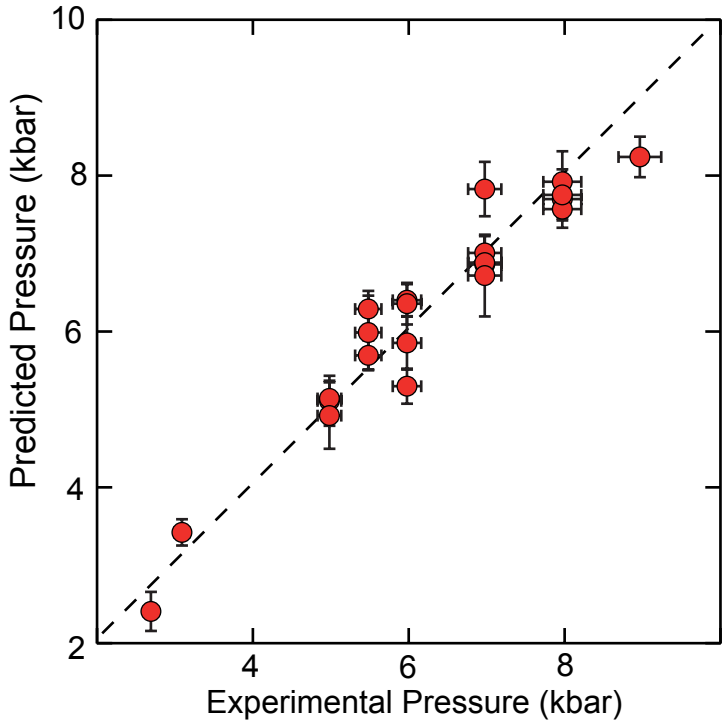

Figure10

Click here to download Figure figure10_rev.pdf

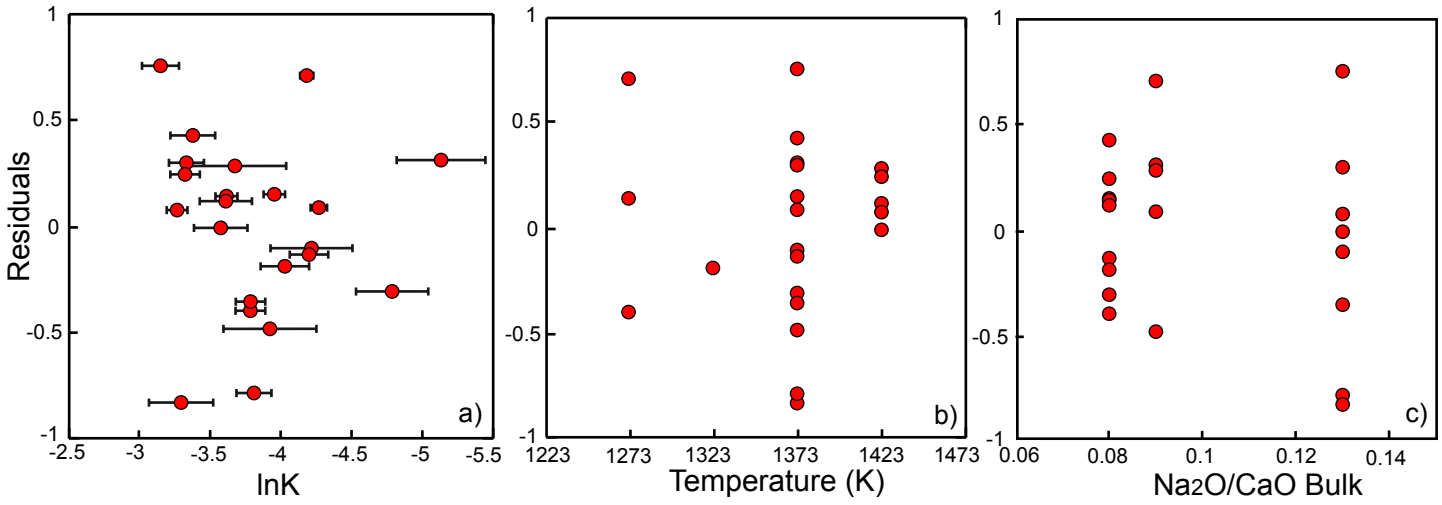

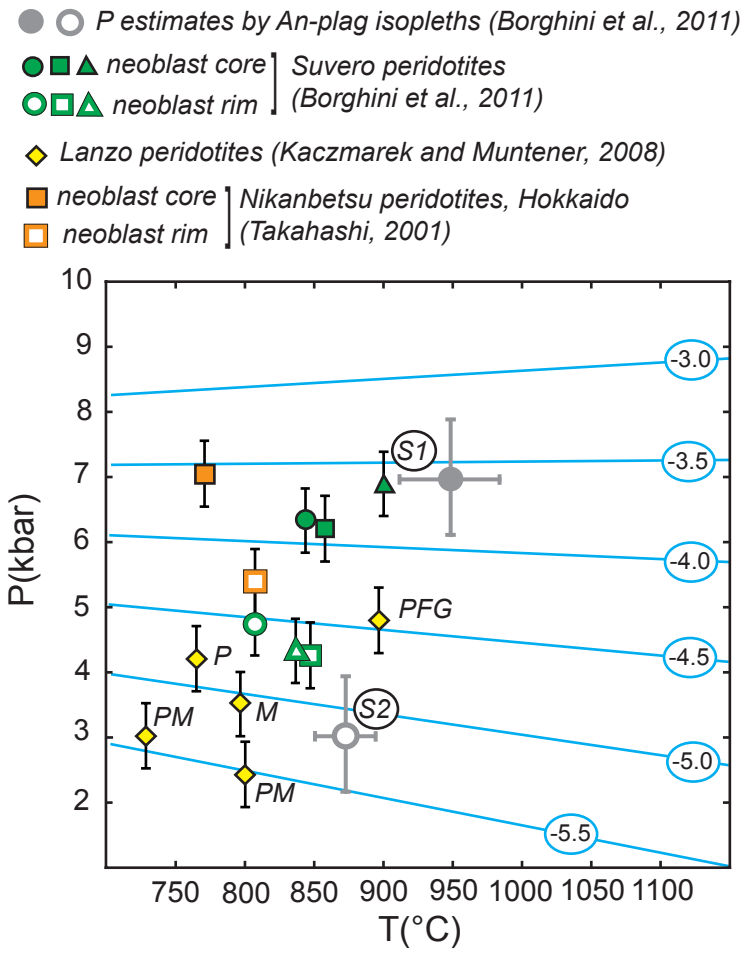

Table 1 Composition of starting materials

wt.%	(1) HNaFLZ -40% ol	(2) FLZ -40% ol	(3) DLZ -40% ol	(4) HNaFLZ	(5) FLZ	(6) DLZ	(7) HPY	(8) MPY	(9) TQ
SiO_2	47.43	47.52	47.52	44.82	44.90	44.90	45.38	44.91	45.15
TiO_2	0.20	0.20	0.14	0.12	0.12	0.07	0.71	0.17	0.08
Al_2O_3	6.30	6.31	3.97	3.78	3.79	2.38	3.55	4.39	3.23
Cr_2O_3	0.68	0.69	0.65	0.41	0.41	0.39	0.43	0.45	0.45
FeO*	6.93	6.96	7.54	7.97	7.99	8.34	8.50	7.58	7.69
MgO	32.06	32.19	36.27	39.05	39.12	41.58	37.63	38.71	40.21
CaO	5.67	5.68	3.56	3.40	3.41	2.14	3.09	3.39	3.00
Na_2O	0.73	0.44	0.34	0.44	0.26	0.20	0.57	0.40	0.18
K_2O	0.00	0.00	0.00	0.00	0.00	0.00	0.13	0.00	0.00
Total	100.00	100.00	100.00	100.00	100.00	100.00	100.00	100.00	100.00
X_{Mg}	0.89	0.89	0.90	0.90	0.90	0.90	0.89	0.90	0.90
X_{Cr}	0.07	0.07	0.10	0.07	0.07	0.10	0.08	0.06	0.09
Na_2O/CaO	0.13	0.08	0.09	0.13	0.08	0.09	0.19	0.12	0.06
Ab/Di (CIPW)	0.23	0.15	0.18	0.23	0.15	0.18	0.30	0.27	0.12

(1), (4): this study; (2), (3), (4), (5), (6): Borghini et al. 2010; (7) HPY: Hawaiian Pyrolite from Green et al. (1979); (8) MPY: “MORB pyrolite” from Green et al. (1979;) (9) TQ: Tinaquillo Peridotite from Green et al. (1979).

Table 2 Run conditions and run products of experiments

RUN	BULK	T (°C)	P (kbar)	Run time (h)	Run products
LC6b	HNa-FLZ	1100	5	672	pl, sp, cpx, opx, ol (amp)
LC1b	HNa-FLZ	1100	5.5	502	pl, sp, cpx, opx, ol (amp)
LC3	HNa-FLZ	1100	6	1002	pl, sp, cpx, opx, ol (amp)
LC4	HNa-FLZ	1050	6.5	290	pl, sp, cpx, opx, ol (amp)
LC2	HNa-FLZ	1100	7	503	pl, sp, cpx, opx, ol (amp)
MP4	HNa-FLZ	1150	7	216	pl, sp, cpx, opx, ol (amp)
MP1	HNa-FLZ	1100	8	88	pl, sp, cpx, opx, ol (amp)
LC7	HNa-FLZ	1150	8	504	pl, sp, cpx, opx, ol (amp)
MP3	HNa-FLZ	1100	9	790	pl, sp, cpx, opx, ol (amp)
MP2	HNa-FLZ	1100	10	480	sp, cpx, opx, ol (amp)
LC1a	DLZ	1100	5.5	502	pl, sp, cpx, opx, ol (amp)
LC5	FLZ	1150	7	504	pl, sp, cpx, opx, ol (amp)

Abbreviations: pl, plagioclase; sp, spinel; cpx, clinopyroxene; opx, orthopyroxene; ol, olivine; amp, parentheses indicate traces

Table 3 Average compositions (wt%) of minerals in experiments

Run	Phase	SiO_2		TiO_2		Al_2O_3		Cr_2O_3		FeO		MgO		CaO		Na_2O		Total	An		X_{Mg}	
MP1	plg(34)	54.94	(0.52)	0.02	(0.02)	29.02	(0.53)	0.03	(0.03)	0.34	(0.05)	0.29	(0.13)	11.57	(0.40)	4.96	(0.21)	101.16	0.563	(0.019)		
	cpx(14)	52.50	(0.40)	0.24	(0.03)	6.40	(0.30)	0.93	(0.10)	3.35	(0.15)	17.30	(0.52)	18.90	(0.73)	0.87	(0.04)	100.49			0.902	(0.002)
	opx(12)	55.30	(0.59)	0.10	(0.02)	5.23	(0.64)	0.60	(0.09)	6.20	(0.10)	31.80	(0.33)	1.54	(0.08)	0.10	(0.01)	100.86			0.901	(0.002)
	ol(11)	41.60	(0.50)	0.01	(0.01)	0.15	(0.16)	0.07	(0.02)	9.82	(0.07)	49.00	(0.41)	0.26	(0.09)	0.01	(0.01)	100.93			0.899	(0.003)
	sp(3)	0.20	(0.35)	0.09	(0.01)	62.40	(0.87)	6.36	(1.35)	8.56	(0.28)	22.00	(0.25)	0.05	(0.05)	0.00	(0.00)	99.66			0.824	(0.006)
	amp(3)	45.80	(0.42)	0.69	(0.03)	14.20	(0.42)	1.03	(0.04)	3.26	(0.08)	19.90	(0.09)	10.60	(0.23)	3.32	(0.08)	98.80	0.638	(0.007)	0.916	(0.003)
MP2	cpx(9)	52.30	(0.49)	0.19	(0.03)	6.68	(0.59)	0.69	(0.20)	3.25	(0.24)	16.90	(0.57)	19.40	(0.54)	1.13	(0.08)	100.54			0.902	(0.005)
	opx(7)	54.10	(0.44)	0.11	(0.04)	5.66	(0.30)	0.56	(0.07)	6.32	(0.11)	30.70	(0.43)	1.64	(0.37)	0.07	(0.03)	99.16			0.896	(0.001)
	ol(5)	40.60	(0.22)	0.00	(0.00)	0.18	(0.04)	0.08	(0.04)	10.00	(0.13)	47.80	(0.16)	0.39	(0.11)	0.00	(0.00)	99.06			0.895	(0.001)
MP3	plg(27)	55.26	(1.31)	0.03	(0.02)	28.83	(0.62)	0.09	(0.07)	0.41	(0.07)	0.47	(0.19)	10.44	(0.45)	5.52	(0.18)	101.04	0.511	(0.018)		
	cpx(10)	52.50	(0.39)	0.20	(0.07)	6.78	(0.40)	0.79	(0.15)	3.20	(0.24)	17.20	(1.18)	18.80	(1.28)	1.05	(0.12)	100.52			0.905	(0.009)
	opx(15)	54.60	(0.58)	0.09	(0.04)	5.57	(0.59)	0.57	(0.05)	6.19	(0.29)	31.70	(0.52)	1.79	(0.47)	0.23	(0.15)	100.74			0.900	(0.002)
	ol(4)	41.10	(0.63)	0.01	(0.01)	0.56	(0.40)	0.10	(0.07)	10.20	(0.15)	49.20	(0.68)	0.30	(0.10)	0.04	(0.04)	101.50			0.896	(0.005)
	sp(3)	0.66	(0.50)	0.04	(0.04)	67.10	(0.89)	1.62	(0.28)	8.19	(0.18)	22.50	(0.08)	0.12	(0.02)	0.00	(0.00)	100.23			0.825	(0.004)
	amp(4)	46.10	(2.07)	0.62	(0.16)	13.40	(1.21)	0.95	(0.14)	3.63	(0.58)	21.40	(2.03)	9.26	(1.85)	3.16	(0.48)	98.52	0.617	(0.016)	0.914	(0.005)
MP4	plg(14)	53.12	(0.80)	0.03	(0.03)	29.76	(0.88)	0.02	(0.01)	0.41	(0.08)	0.42	(0.14)	12.66	(0.68)	4.12	(0.41)	100.54	0.630	(0.036)		
	cpx(18)	51.90	(0.52)	0.29	(0.06)	5.92	(0.51)	1.09	(0.05)	3.34	(0.27)	18.20	(0.83)	18.40	(0.74)	0.61	(0.03)	99.75			0.906	(0.007)
	opx(10)	54.80	(0.33)	0.14	(0.03)	4.90	(0.64)	0.73	(0.11)	5.75	(0.35)	32.00	(0.54)	1.77	(0.23)	0.09	(0.02)	100.18			0.908	(0.006)
	ol(9)	41.00	(0.22)	0.02	(0.03)	0.28	(0.20)	0.12	(0.04)	9.23	(0.46)	48.90	(0.85)	0.36	(0.17)	0.03	(0.02)	99.94			0.904	(0.009)
	amp(8)	45.40	(0.71)	0.64	(0.09)	13.60	(0.53)	1.12	(0.13)	3.01	(0.16)	21.40	(0.76)	10.80	(0.41)	3.11	(0.17)	99.08	0.657	(0.008)	0.927	(0.002)
LC1b	plg(9)	50.75	(1.15)	0.05	(0.05)	31.70	(1.17)	0.05	(0.06)	0.08	(0.07)	0.05	(0.06)	13.72	(0.21)	3.85	(0.12)	100.26	0.663	(0.009)		
	cpx(8)	51.70	(0.55)	0.24	(0.04)	5.14	(0.38)	0.84	(0.09)	3.22	(0.25)	18.10	(0.51)	20.00	(0.83)	0.49	(0.09)	99.72			0.909	(0.006)
	opx(14)	55.40	(0.48)	0.14	(0.04)	4.13	(0.85)	0.66	(0.06)	6.49	(0.25)	31.70	(0.63)	1.91	(0.35)	0.11	(0.06)	100.53			0.897	(0.004)
	amp(7)	46.20	(1.13)	0.49	(0.13)	11.50	(0.86)	1.02	(0.10)	3.18	(0.24)	23.40	(1.84)	9.84	(0.91)	2.61	(0.43)	98.24	0.677	(0.022)	0.929	(0.005)
LC2	plg(7)	51.01	(1.58)	0.02	(0.03)	31.66	(1.29)	0.14	(0.21)	0.11	(0.16)	0.00	(0.00)	12.84	(0.81)	4.38	(0.36)	100.16	0.618	(0.030)		
	cpx(10)	51.30	(0.59)	0.24	(0.04)	6.36	(0.59)	0.78	(0.20)	2.99	(0.19)	16.60	(0.51)	20.70	(0.80)	0.60	(0.11)	99.57			0.908	(0.004)
	opx(5)	54.90	(0.31)	0.11	(0.05)	4.39	(0.94)	0.64	(0.15)	6.71	(0.90)	31.20	(0.62)	1.62	(0.14)	0.12	(0.06)	99.69			0.892	(0.014)

	ol(6)	40.80	(0.33)	0.00	(0.00)	0.38	(0.25)	0.10	(0.11)	9.99	(0.17)	47.90	(0.23)	0.27	(0.05)	0.01	(0.02)	99.45			0.896	(0.006)
	amp(4)	44.30	(1.20)	0.74	(0.26)	13.00	(0.78)	0.95	(0.29)	3.38	(0.53)	21.90	(1.87)	10.20	(0.89)	2.88	(0.21)	97.35	0.661	(0.026)	0.920	(0.011)
LC3	plg(30)	50.76	(1.07)	0.03	(0.03)	31.13	(0.99)	0.03	(0.03)	0.33	(0.10)	0.18	(0.23)	13.89	(0.80)	3.48	(0.40)	99.82	0.688	(0.037)		
	cpx(10)	51.80	(0.38)	0.25	(0.05)	5.19	(0.23)	1.09	(0.10)	3.04	(0.12)	17.50	(0.17)	20.30	(0.33)	0.49	(0.03)	99.66			0.911	(0.003)
	opx(9)	54.90	(0.59)	0.11	(0.03)	4.29	(0.55)	0.72	(0.09)	5.95	(0.08)	32.30	(0.35)	1.61	(0.13)	0.07	(0.02)	99.94			0.906	(0.001)
	ol(8)	40.60	(0.27)	0.02	(0.02)	0.11	(0.08)	0.08	(0.05)	9.54	(0.15)	49.40	(0.21)	0.21	(0.03)	0.01	(0.01)	99.96			0.902	(0.002)
	sp(6)	0.47	(0.29)	0.11	(0.05)	48.30	(0.70)	22.20	(0.53)	9.97	(0.10)	19.40	(0.16)	0.14	(0.04)	0.00	(0.00)	100.59			0.771	(0.002)
	amp(10)	43.90	(0.34)	0.72	(0.05)	14.20	(0.17)	1.58	(0.09)	3.00	(0.06)	19.30	(0.15)	11.20	(0.05)	3.04	(0.07)	96.94	0.670	(0.005)	0.920	(0.001)
LC6b	plg(14)	51.18	(0.42)	0.04	(0.02)	30.65	(0.33)	0.05	(0.04)	0.18	(0.08)	0.11	(0.05)	14.18	(0.29)	3.45	(0.15)	99.84	0.694	(0.014)		
	cpx(11)	52.00	(1.11)	0.26	(0.07)	4.25	(0.64)	1.03	(0.22)	3.19	(0.12)	18.90	(0.48)	19.40	(0.25)	0.45	(0.07)	99.48			0.913	(0.004)
	opx(10)	55.70	(0.74)	0.13	(0.04)	3.43	(0.68)	0.68	(0.10)	6.37	(0.23)	32.00	(0.45)	1.77	(0.15)	0.09	(0.05)	100.16			0.900	(0.003)
	ol(13)	40.40	(0.38)	0.04	(0.03)	0.43	(0.25)	0.27	(0.15)	10.10	(0.39)	48.20	(0.79)	0.30	(0.18)	0.04	(0.06)	99.77			0.894	(0.008)
	amp(6)	45.60	(0.76)	0.59	(0.09)	11.90	(0.67)	1.23	(0.12)	2.57	(0.31)	22.40	(1.50)	10.90	(0.69)	2.88	(0.25)	98.07	0.677	(0.011)	0.939	(0.008)
LC7	plg(6)	54.30	(0.32)	0.01	(0.01)	29.42	(0.16)	0.01	(0.01)	0.23	(0.07)	0.14	(0.05)	11.56	(0.11)	5.08	(0.09)	100.75	0.557	(0.007)		
	cpx(3)	51.10	(0.34)	0.35	(0.09)	6.33	(0.25)	0.94	(0.09)	3.26	(0.15)	17.50	(0.45)	19.20	(0.50)	0.64	(0.05)	99.32			0.905	(0.004)
	opx(14)	54.50	(0.63)	0.10	(0.03)	4.87	(0.90)	0.71	(0.12)	6.19	(0.46)	31.20	(0.34)	1.82	(0.31)	0.11	(0.05)	99.50			0.900	(0.007)
	ol(5)	41.20	(1.11)	0.03	(0.02)	0.99	(0.18)	0.25	(0.10)	9.77	(0.21)	47.20	(0.32)	0.54	(0.18)	0.06	(0.02)	100.03			0.896	(0.004)
	amp(11)	45.60	(1.36)	0.57	(0.10)	12.00	(0.94)	0.90	(0.09)	3.21	(0.30)	22.00	(1.00)	9.48	(0.89)	3.06	(0.24)	96.83	0.631	(0.014)	0.924	(0.004)
LC1a	plg(10)	48.36	(2.16)	0.08	(0.16)	33.34	(2.23)	0.08	(0.15)	0.17	(0.09)	0.11	(0.12)	14.61	(0.54)	3.36	(0.20)	100.11	0.706	(0.019)		
	cpx(13)	52.00	(0.71)	0.26	(0.14)	4.83	(0.67)	0.68	(0.09)	3.32	(0.57)	17.70	(0.94)	20.70	(1.21)	0.41	(0.09)	99.89			0.905	(0.011)
	opx(10)	55.30	(0.71)	0.14	(0.05)	3.50	(0.39)	0.62	(0.07)	6.78	(0.26)	32.00	(0.49)	1.77	(0.30)	0.09	(0.04)	100.20			0.894	(0.003)
	ol(5)	41.10	(0.14)	0.02	(0.02)	0.44	(0.21)	0.11	(0.05)	10.30	(0.42)	47.60	(0.41)	0.39	(0.09)	0.03	(0.04)	99.99			0.892	(0.007)
	amp(7)	44.70	(0.60)	3.04	(0.53)	10.90	(0.61)	1.13	(0.09)	3.63	(0.28)	20.90	(0.94)	10.50	(0.46)	2.89	(0.11)	97.69	0.668	(0.010)	0.911	(0.004)
LC5	plg(27)	51.01	(1.03)	0.03	(0.02)	31.21	(0.76)	0.04	(0.03)	0.41	(0.07)	0.42	(0.20)	13.62	(0.54)	3.55	(0.32)	100.30	0.685	(0.031)		
	cpx(10)	50.70	(0.42)	0.63	(0.09)	5.85	(0.52)	1.11	(0.09)	3.58	(0.07)	17.50	(0.49)	19.20	(0.36)	0.54	(0.05)	99.11			0.897	(0.002)
	opx(10)	53.70	(0.57)	0.23	(0.07)	5.05	(0.66)	0.80	(0.07)	6.51	(0.27)	31.20	(0.39)	2.01	(0.19)	0.07	(0.02)	99.58			0.895	(0.004)
	ol(6)	40.10	(0.58)	0.05	(0.03)	0.51	(0.34)	0.20	(0.13)	10.60	(0.12)	47.60	(0.44)	0.45	(0.15)	0.04	(0.02)	99.55			0.889	(0.007)

Mineral abbreviations are as in Table 2. An= Ca/(Ca+Na). Along with the phase, we report the number of analyses in parentheses. Numbers in parentheses correspond to 1σ standard deviations.

Table 4 Averaged values of end member activities in minerals used to compute lnK of the reaction FACE

P (kbar)	T(°C)	Bulk	acats		aen		XAn,C		afo		lnK	
5.0	1373	HNaFLZ	0.0122	(0.0035)	0.7455	(0.0092)	0.7723	(0.0143)	0.7998	(0.0074)	-4.2182	(0.2893)
5.5	1373	HNaFLZ	0.0179	(0.0022)	0.7327	(0.0145)	0.7394	(0.0094)	0.7998	(0.0074)	-3.8114	(0.1233)
6.0	1373	HNaFLZ	0.0184	(0.0017)	0.7529	(0.0069)	0.7525	(0.0374)	0.8141	(0.0025)	-3.7893	(0.1041)
7.0	1373	HNaFLZ	0.0283	(0.0062)	0.7263	(0.0203)	0.6911	(0.0323)	0.8016	(0.0035)	-3.2941	(0.2264)
7.0	1423	HNaFLZ	0.0213	(0.0038)	0.7477	(0.0113)	0.6967	(0.0377)	0.8177	(0.0097)	-3.5771	(0.1888)
8.0	1373	HNaFLZ	0.0247	(0.0029)	0.7373	(0.0079)	0.6324	(0.0199)	0.8080	(0.0014)	-3.3343	(0.1234)
8.0	1423	HNaFLZ	0.0258	(0.0018)	0.7308	(0.0088)	0.6174	(0.0072)	0.8029	(0.0031)	-3.2691	(0.0730)
9.0	1373	HNaFLZ	0.0271	(0.0034)	0.7254	(0.0132)	0.5766	(0.0194)	0.8026	(0.0011)	-3.1588	(0.1303)
7.0	1423	FLZ	0.0221	(0.0040)	0.7207	(0.0098)	0.7466	(0.0200)	0.7904	(0.0083)	-3.6123	(0.1833)
5.5	1373	DLZ	0.0167	(0.0055)	0.7360	(0.0080)	0.7849	(0.0328)	0.7956	(0.0020)	-3.9280	(0.3279)
Borghini et al. 2010												
3.1	1373	FLZ	0.0080	(0.0020)	0.7493	(0.0039)	0.9072	(0.0118)	0.7889	(0.0014)	-4.7837	(0.2551)
5.0	1373	FLZ	0.0135	(0.0018)	0.7388	(0.0060)	0.8382	(0.0220)	0.7902	(0.0054)	-4.1958	(0.1359)
6.0	1273	FLZ	0.0186	(0.0019)	0.7392	(0.0063)	0.7655	(0.0169)	0.7964	(0.0019)	-3.7919	(0.1046)
6.0	1373	FLZ	0.0157	(0.0010)	0.7380	(0.0057)	0.7651	(0.0287)	0.7888	(0.0065)	-3.9529	(0.0757)
7.0	1273	FLZ	0.0206	(0.0016)	0.7372	(0.0010)	0.7189	(0.0048)	0.7915	(0.0032)	-3.6236	(0.0772)
8.0	1373	FLZ	0.0246	(0.0037)	0.7244	(0.0093)	0.6620	(0.0265)	0.7937	(0.0076)	-3.3839	(0.1574)
2.7	1373	DLZ	0.0058	(0.0018)	0.7611	(0.0055)	0.9207	(0.0461)	0.8168	(0.0024)	-5.1379	(0.3131)
5.0	1373	DLZ	0.0127	(0.0005)	0.7430	(0.0040)	0.8547	(0.0352)	0.7905	(0.0036)	-4.2711	(0.0581)
6.0	1273	DLZ	0.0127	(0.0006)	0.7537	(0.0031)	0.7900	(0.0062)	0.8041	(0.0013)	-4.1951	(0.0468)
7.0	1423	DLZ	0.0202	(0.0073)	0.7409	(0.0052)	0.7472	(0.0273)	0.7903	(0.0038)	-3.6753	(0.3617)
Borghini et al. 2011												
5.5	1323	FLZ	0.0156	(0.0026)	0.7386	(0.0040)	0.8121	(0.0381)	0.7933	(0.0049)	-4.0238	(0.1709)
0.8	1423	FLZ	0.0264	(0.0018)	0.7265	(0.0067)	0.6734	(0.0124)	0.7902	(0.0036)	-3.3247	(0.1037)

Numbers in parentheses correspond to 1σ standard deviations, errors in lnK have been propagated from activities uncertainties.

Dear Othmar,

Please find enclosed the revised version of the t manuscript entitled "Experimental calibration of Forsterite-Anorthite-CaTschermak-Enstatite (FACE) geobarometer for mantle peridotites" submitted for publication to Contributions to Mineralogy and Petrology.

The manuscript has been revised and improved, according to the reviewers and editorial comments. The main issue needing attention was the **activity model in clinopyroxene**, and the way we calculate Al(IV). In agreement with Reviewer #2, we calculate the Al(IV) of clinopyroxene as (Al+Cr+2Ti –Na). We also adopted this approach for calculating Al(IV) and Al(VI) in orthopyroxene. Using the new evaluation of activities, we performed again the calibration and we modified figures, tables and text accordingly.
As expected, this change has minor importance for the calibration and does not substantially influence our results. As an example, in the estimate of pressure for Suvero peridotites we determined in the previous version 6.2 and 6.9 kbar that have changed to 6.3 and 7.0 kbar.

All other minor suggestions, including your editorial changes, have been carefully taken into account. The very minor suggestions are not listed in the following as they were simply taken into consideration, adding appropriate sentences and/or modifying the text in order to make it clearer. We list therefore only minor comments that deserve more explanation.

Reviewer # 1

The major issue raised by Reviewer#1 is the last comment on Figure 11 and the T dependence of isopleths of lnK. A direct comparison between these lines (i.e. isopleths of lnK= ln ($a_{Ca\text{-}Ts}$ *a_{en} / a_{fo} *a_{an}) and those in the CMAS system reported by Herzberg (1978) is not straightforward, as the isopleths in figure 6, Herzberg, 1978 refer to K= (X_{Mg}^{M2} * X_{Mg}^{M1}) in cpx/(X_{Mg}^{M2} * X_{Mg}^{M1}) in opx defined for the equilibirum opx<->cpx). In any case, the T dependence of lnK for the present study has been discussed in the application of the FACE geobarometer.

Reviewer #2

In addition to the main issue about the activity of pyroxene above described, Reviewer #2 raised two other major issues:

1. p. 16 line 43+: equilibrium between neoblastic cores of different minerals.
   We agree that, if zoning profiles suggest Ab loss of plagioclase cores, the equilibrium assumption is lost for the cores. In this case the application of the geobarometer could give a minimum estimate of pressure. However this comment is mostly related to a published paper (Borghini et al. 2011) and the issue is beyond the scope of the present manuscript.

2. p. 16-17: Nimis and Gruetter (2010) showed that the two-px thermometer of Brey and Koehler (1990) is less robust than that of Taylor (1998), especially for high-Na compositions.
   We took this into account and adopt the Taylor (1998) geothermometer as a reference geothermometer to apply the FACE geobarometer. We therefore modify Figure 11 and the related Supplementary Figure 2s. Following the suggestion of the reviewer we compared the result of the FACE geobarometer considering Taylor and Ca-in-opx geothermometer of Brey and Koelher (1990).

Other minors comments are commented as follow:

p. 6 lines 7+: We added a sentence at page 6 discussing how the P-T range of the calibration experiments compares with P-T estimates expected in natural plagioclase peridotites.

p. 9: Fig5a and b. We added few sentences on this comment on the slight differences in Al vs P diagram between pyroxenes of depleted and fertile peridotites.

p. 10 bottom: confusion in the use of the term 'depletion'. We agree, the term “depletion” was misused and we modified the text accordingly.

p. 12 line 16: meaning of the A, B and C parameters. We modified the text in order to clarify that we do not fit any thermodynamic parameters.

p. 12 bottom: "Based on the phase diagram of C&McC (1984), without considering the effect of pressure,…". It is unclear whether the original phase diagram did or did not include an effect of P. However, on which basis can this effect be neglected?

We agree. Our choice is motivated by the fact that our data span a wide range of composition and temperatures where the transition has been observed. However, in the C&McC (1984) diagram no effect of pressure on the c1 to I1 transition is considered. No data on the combined effect of both P and T are available, at least in the pressure range of interest (P< 10 kbar). As a result the effect of pressure on the C1 to I1 transition cannot be evaluated and incorporated in an activity model. Since we are not fitting thermodynamic parameters, we adopt the same procedure followed in previous geobarometer calibration involving plagioclase McCarthy and Patiño Douce (1998).

As we said before, we followed your editorial suggestions included in your marked manuscript. However we did not compare the location of plagioclase to spinel transition with data on solidus reported by Till et al. (2012) as we think that they are not directly comparable. The bulk composition investigated by Till et al. 2012 does not include Cr and additionally presents a Na_2O/CaO ratio of about 0.3, much higher than our most enriched bulk composition. Furthermore the transition is not well constrained as they report plagioclase up to 10 kbar and both plagioclase and spinel absent assemblage at 14 kbar, at 1270°C.

We think to have properly addressed all major comments and suggestions raised by the reviewers, and we believe the paper has benefited of this revision.

We hope to have been sufficiently clear in explaining how we managed the reviewer and editorial comments, and remain at your disposal for any further request of clarification.

Best regards.
Patrizia

figure1s

figure2s

spreadsheet

Click here to access/download

Electronic supplementary material

spreadsheet_geobarPI_revision.xlsx